1.05 Theory and Observations – Forward Modeling/Synthetic Body Wave Seismograms

V. F. Cormier, University of Connecticut, Storrs, CT, USA

1.05.1 Introduction

Body waves are solutions of the elastic equation of motion that propagate outward from a seismic source in expanding, quasi-spherical wave fronts, much like the rings seen when a rock is thrown in a pond. The normals to the wave fronts, called rays, are useful in the illustrating body waves' interactions with gradients and discontinuities in elastic velocities and as well as their sense of polarization of particle motion. Except for the special cases of grazing incidence to discontinuities, body-wave solutions to the equations of motion are nearly nondispersive. All frequencies propagate at nearly the same phase and group velocities. Hence the body wave excited by an impulsive, delta-like, seismic source-time function will retain its delta-like shape with propagation to great distances (**Figure 1**).

Surface waves are solutions of the elastic equations of motion that exponentially decay with depth beneath the surface of the Earth for a boundary condition of vanishing stress at the surface (*see* Chapter 1.02). Unlike body waves, surface waves are strongly

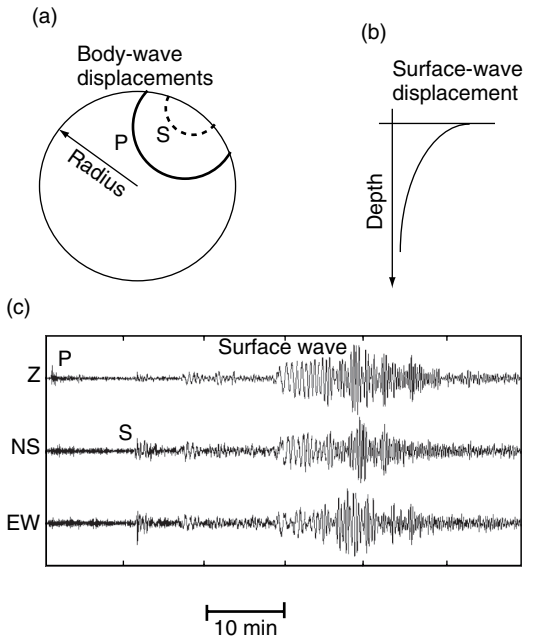

Figure 1 (a) Displacement of body waves is concentrated in propagating quasi-spherical wave fronts. (b) The displacement of surface waves exponentially decays away from the surface of the Earth. (c) Example seismogram showing implusive, pulse-like, body waves and dispersive surface waves.

dispersed in the Earth, having phase and group velocities that depend on frequency. Observations of surface waves in the 0.001–0.1 Hz band of frequencies can constrain structure of the crust and upper mantle of the Earth, but only body waves provide information on the elastic velocities of the deeper interior of the Earth, all the way to its center. Summing modes of free oscillation of the Earth can represent both body and surface waves. The most efficient representation of the highest frequency content body waves, however, is given by propagating wave front or ray-type solutions of the elastic equations.

In a homogeneous Earth, the wave fronts of body waves are spherical, with radii equal to the distance from the source to an observation point on the wave front. Since the density of kinetic energy at a point in time is simply the surface area of the wave front, the particle velocity of a body wave is inversely proportional to the distance to the source. This inverse scaling of amplitude with increasing distance is termed the geometric spreading factor, R. Even in an inhomogeneous Earth, the inverse-distance scaling of body-wave amplitude can be used to make a rough estimate of the behavior of amplitude versus distance.

Rays follow paths of least or extremal time, representing a stationary phase approximation to a solution of a wave equation, Fourier-transformed in space and time. The least-time principle is expressed by Snell's law. In spherical geometry and radially varying velocity, Snell's law is equivalent to the constancy of a ray parameter or horizontal slowness p. The ray parameter is defined by $p = r\,\sin(i)/v(r)$, where i is the acute angle between the intersection of a ray path and a surface of radius r, and v is the body-wave velocity. Snell's law is obeyed by ray paths in regions of continuously varying velocity as well as by the ray paths of reflected and transmitted/converted waves excited at discontinuities. Since velocities usually increase with depth (decrease with radius) in the Earth, ray paths of body waves are usually concave upward (**Figure 2**). The least-time principle can also be exploited in linearized tomography to find perturbations to reference Earth models by assuming that ray paths are stationary with respect to small perturbations in velocities.

Complementing the information contained in travel times are the shapes (waveforms) of the body waves. Complexities and subtle shape changes observed in waveforms can be used to image elastic properties of the Earth at spatial scales down to a quarter wavelength from its surface to its center. The velocities of body waves in the Earth range from $1.5\,\mathrm{km\,s^{-1}}$ to greater than $13\,\mathrm{km\,s^{-1}}$. Since waves that penetrate the deep interior of the Earth are commonly observed at frequencies at least up to 2 Hz, structure having spatial scales as small as 1 km can be potentially imaged from a densely sampled wavefield. Body waveforms also contain information about the spatial and temporal history of earthquake, explosion, or impact seismic sources.

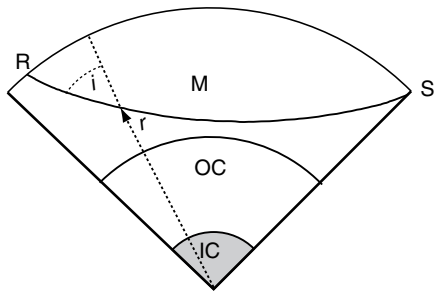

Figure 2 Following Snell's law in spherical geometry ($r\,\sin(i)/v$ = constant), the ray paths of body waves in the Earth are mostly concave upward because elastic velocities mostly increase with depth.

This chapter reviews algorithms for modeling the effects of structure and source on teleseismic waveforms (*see* Chapter 1.22). It will point to references for the theoretical background of each algorithm and currently existing software. It will also make suggestions for the model parametrization appropriate to each algorithm, and the treatment of source-time functions, instrument responses, attenuation, and scattering. Mathematical development of each algorithm can be found in textbooks in advanced and computational seismology (Dahlen and Tromp, 1998; Aki and Richards, 1980, 2002; Kennett, 1983, 2001; Cerveny, 2001; Chapman, 2004). A thorough understanding of the derivation of each algorithm requires a background that includes solution of partial differential equations by separation of variables, special functions, integral transforms, complex variables and contour integration, and linear algebra. Practical use of each algorithm, however, often requires no more than a background in simple calculus and an intuitive understanding how a wavefield can be represented by superposing either wave fronts or modes at different frequencies.

1.05.2 Plane-Wave Modeling

1.05.2.1 Elastic Velocities and Polarizations

Two types of body waves were identified in early observational seismology, P, or primary, for the first arriving impulsive wave and S, or secondary, for a second slower impulsive wave (Bullen and Bolt, 1985). These are the elastic-wave types that propagate in an isotropic solid. In most regions of the Earth, elasticity can be well approximated by isotropy, in which only two elastic constants are required to describe a stress–strain relation that is independent of the choice of the coordinate system. In the case of anisotropy, additional elastic constants are required to describe the stress–strain relation. In a general anisotropic solid, there are three possible body-wave types, P, and two quasi-S waves, each having a different velocity.

The velocities of propagation and polarizations of motion of P and S waves can be derived from elastic equation of motion for an infinitesimal volume in a continuum:

$$\rho \frac{\partial^2 u_i}{\partial t^2} = +\sigma_{ij,j} = -f_i \qquad [1]$$

where ρ is density, u_i is the ith component of the particle displacement vector $\mathbf{U}$, σ_{ij} is the stress tensor, and f_i is the ith component of body force that excites elastic motion. The elastic contact force in the ith direction is represented by the jth spatial derivative of the stress tensor, $\sigma_{ij,j}$. The stress tensor elements are related to spatial derivatives of displacement components (strains) by Hooke's law, which for general anisotropy takes the form

$$\sigma_{ij} = c_{ijkl}\, u_{k,l} \qquad [2]$$

and for isotropy the form

$$\sigma_{ij} = \lambda \frac{\partial u_i}{\partial x_i} + \mu \left(\frac{\partial u_i}{\partial x_j} + \frac{\partial u_j}{\partial x_i} \right) \qquad [3]$$

where c_{ijkl}, λ, and μ are elastic constants. The summation convention is assumed in [1]–[3], that is, quantities are summed over repeated indices.

Elastic-wave equations for P and S waves can be derived by respectively taking the divergence and curl of the equation of motion [11], demonstrating that volumetric strain, $\nabla \cdot U$, propagates with a P-wave velocity,

$$V_P = \sqrt{\frac{\lambda + 2\mu}{\rho}} = \sqrt{\frac{K + 4/3\mu}{\rho}} \qquad [4a]$$

and rotational strain, $\nabla \times U$, propagates with the S-wave velocity,

$$V_S = \sqrt{\frac{\mu}{\rho}} \qquad [4b]$$

Note that the P-wave velocity can be represented in terms of either the Lame parameter λ and shear modulus μ or the bulk modulus K and shear modulus μ.

Alternatively, the phase velocities and polarizations of body waves can be derived by assuming propagation of a plane wave having frequency ω and a normal $\mathbf{k}$ of the form

$$\mathbf{U}(\mathbf{x}, t) = \mathbf{A} e^{(i\omega t - \mathbf{k} \bullet \mathbf{x})} \qquad [5]$$

and substituting this form into [1]. This substitution leads to an eigenvalue/eigenvector problem, in which the eigenvalues represent the magnitudes of the wavenumber vector $\mathbf{k}$, and hence phase velocities from $v = \omega/|\mathbf{k}|$. The associated eigenvectors represent the possible orientations of particle motion (e.g., Keith and Crampin, 1977). For propagation in three dimensions (3-D), there are three possible eigenvalues/eigenvectors, two of which are equal or degenerate in an isotropic medium. The eigenvalue

with the fastest phase velocity is the P wave. It has an eigenvector or polarization that is in the direction of the P ray, normal to the wave front. In an isotropic medium, the two degenerate eigenvalues and their eigenvectors are associated with the S wave. Their eigenvectors of polarization are perpendicular to the S ray, tangent to the wave front.

To facilitate the solution and understanding of the interactions of the P- and S-wave types with discontinuities in elastic moduli and/or density, it is convenient to define a ray (sagittal) plane containing the source, receiver, and center of the Earth. In an isotropic medium, the S polarization, which depends on the details of source excitation and receiver azimuth, is decomposed into an SV component, lying in the sagittal plane, and an SH component, perpendicular to the sagittal plane (**Figure 3**). At a discontinuity in elastic velocity, SV waves can excite converted–transmitted and reflected P waves and vice versa, but SH waves can only excite transmitted and reflected SH waves. The effects of body-wave-type conversions on polarizations have contributed to fundamental discoveries in deep Earth structure. The most famous example of these discoveries is the SV polarization of the SKS wave, which confirms that the outer core of the Earth is liquid. In this example, the SV component of an S wave incident on the boundary of the solid mantle excites a converted–transmitted P wave in the liquid outer core (K wave), which can convert back to an SV wave in the solid mantle. The SH component of the incident S wave cannot excite a K wave in the liquid

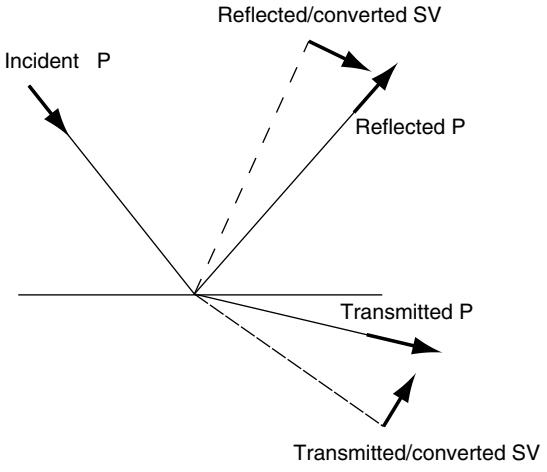

Figure 3 The interaction of a P wave incident on a discontinuity in P and S velocity, showing reflected and converted P and SV waves and their polarizations (arrows).

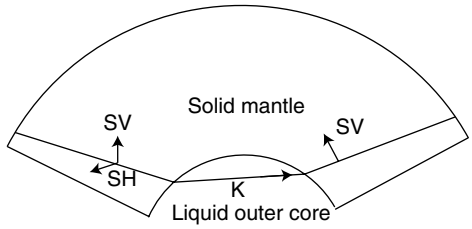

Figure 4 The SV component of the S wave on core–mantle boundary excites a compressional (K) wave in the outer core, which has its particle motion along its ray. The K wave exits the outer core as a transmitted SV wave in the mantle, which has its particle motion perpendicular to its ray, lying in the sagittal plane.

outer core, and hence the received SKS wave is purely SV polarized in an isotropic Earth (**Figure 4**).

Solutions of the elastic equations of motions can also be developed in terms of potentials, showing that the existence of fully decoupled P- and S-wave equations exist only in homogeneous regions where elastic moduli and density are constant in space (e.g., Aki and Richards, 2001). The use of potentials, however, leads to needless mathematical complexity when the quantities of modeling interest are displacements and stresses. This is especially true when solutions are continued across discontinuities in elastic moduli and density. At discontinuities, boundary conditions must be imposed on components u_i of the particle displacement vector **U** and stress tensor elements σ_{ij}. Three fundamental types of boundary conditions occur in seismic wave propagation in the Earth: (1) the surface of the Earth, where all elements σ_{ij} vanish; (2) welded, slip-free, discontinuities between two solid discontinuities, where both particle displacements and stress tensor elements are continuous; and (3) liquid–solid discontinuities such as the ocean/ocean crust, mantle/outer core, and outer core/inner core, where only the displacements and stresses perpendicular to the discontinuity are continuous (*see* Chapter 1.19). These boundary conditions and the associated changes in the eigenvectors and eigenvalues of plane-wave solutions can be compactly handled by a fundamental matrix and propagator formalism (Gilbert and Backus, 1966). In this approach, the vertically separated component for the solution to the equations of motion is written as a linear system of the type:

$$\frac{\mathrm{d}\mathbf{f}}{\mathrm{d}z} = \mathbf{A}\mathbf{f} \qquad [6]$$

where **f** is a 2-vector for the components of displacement and stress associated with SH waves or a

4-vector for the components of stress and displacement associated with P and SV waves; **A** is either a 2×2 matrix for SH waves or a 4×4 matrix for P and SV waves; and derivative d/dz is with respect to depth or radius. The possibility of both up- and down-going waves allows the most general solution of the linear system in eqn [6] to be written as a solution for a fundamental matrix **F**, where the rows of **F** are the components of displacement and stress and the columns correspond to up- and down-going P and S waves. For P and SV waves, **F** is a 4×4 matrix; for SH waves, F is a 2×2 matrix. An example of the fundamental matrix for SH waves in a homogeneous layer is

$$\mathbf{F} = \begin{pmatrix} e^{i\omega k_z(z-z_o)} & e^{-i\omega k_z(z-z_o)} \\ ik_z\mu e^{i\omega k_z(z-z_o)} & -ik_z\mu e^{-i\omega k_z(z-z_o)} \end{pmatrix} \qquad [7]$$

where z_o is the reference depth, and the sign of the complex phasors represents propagation with or against the z-axis to describe down- or up-going waves.

The solution of [6] can be continued across discontinuities, with all boundary conditions satisfied, by use of a propagator matrix **P**, where **P** also satisfies [6]. The fundamental matrix in layer 0 at depth z_1, $\mathbf{F}_o(z_1)$, is related to the fundamental matrix in layer N at z_N, $\mathbf{F}_N(z_N)$, through a propagator matrix $\mathbf{P}(z_1, z_N)$ such that

$$\mathbf{F}_o(z_1) = \mathbf{P}(z_1, z_N)\mathbf{F}_N(z_N) \qquad [8a]$$

where

$$\mathbf{P}(z_1, z_N) = (\mathbf{F}_1(z_1)\mathbf{F}_1^{-1}(z_2))(\mathbf{F}_2(z_2)\mathbf{F}_2^{-1}(z_3))\cdots \times (\mathbf{F}_{N-1}(z_{N-1})\mathbf{F}_{N-1}^{-1}(z_N)) \qquad [8b]$$

In an isotropic Earth model, once the relative source excitation of S waves has been resolved into separate SH and SV components of polarization, the treatment of boundary conditions on P and SV waves can be separated from that needed for SH waves by the use of the either the 4×4 fundamental matrices for P and SV waves or the 2×2 fundamental matrices for SH waves.

1.05.2.2 Superposition of Plane Waves

Superposition of plane waves of the form in [5] along with techniques of satisfying boundary conditions at discontinuities using fundamental and propagator matrix solutions of [8a] and [8b] allow calculation of all possible body-wave solutions of the elastic equations of motion as well as the dispersive-wave interactions with the free surface (surface waves) and deeper discontinuities (diffractions and head waves). This process of superposition in space and frequency is equivalent to solution of the equations of motion by the integral transform methods of Fourier, Laplace, Bessel, or spherical harmonics. Fourier and Laplace transforms can always be applied in a Cartesian coordinate system, but analytic solutions of the equation of motion in terms of Bessel/Hankel and spherical harmonics is limited to Earth models whose layers and discontinuities are either spherically symmetric or plane-layered, having cylindrical symmetry about the source point. Some well-tested extensions and perturbation methods, however, allow their application to models in which the symmetry is broken by lateral heterogeneity, aspherical or nonplanar boundaries, and anisotropy.

Transform-based methods, ray-based methods, and their extensions are reviewed in Section 1.05.4. Before beginning this review, however, it is important to have an intuitive feel for the effects of the Earth structure on the propagation of body waves, how structure can induce complexity in body waveforms, and what outstanding problems can be investigated by the synthesis of waveforms.

1.05.3 Structural Effects

1.05.3.1 Common Structural Effects on Waveforms

Body waves are commonly synthesized to study the effects of waveform complexity or multipathing due to rapid or discontinuous changes in elastic velocity. Two common structures inducing waveform complexity are a rapid or discontinuous velocity decrease and a rapid or discontinuous velocity decrease (**Figure 5**). A rapid or discontinuous decrease is characterized by a shadow zone, followed by a caustic and two multipaths in the lit zone, each having opposite sign of curvature in their associated traveltime curves. A caustic is a surface, line, or point where body waves are strongly focused, frequency-independent ray theory breaks down, and geometric spreading vanishes. A rapid or discontinuous velocity increase produces a triplication of the traveltime curve, with a region of distances in which three different ray paths, one of which has an opposite sign of curvature in its traveltime curve compared to those of the other two paths. The two points where the curvature of traveltime versus distance changes

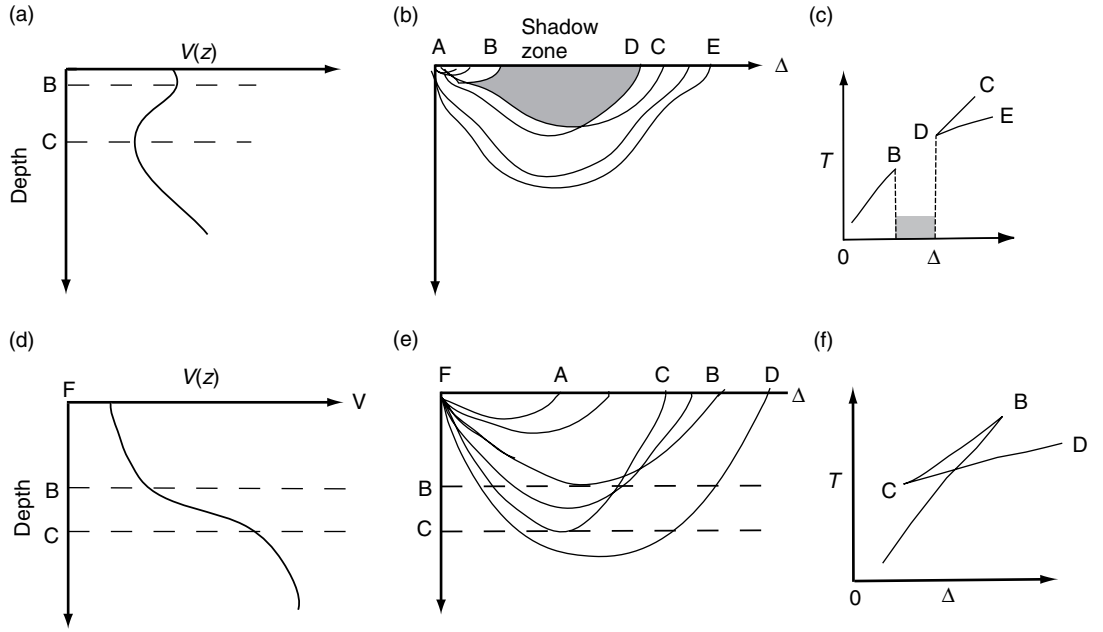

Figure 5 Ray multipathing and traveltime complexity induced by a regions of either rapid velocity decrease with depth ((a)–(c)) or rapid increase ((d)–(f)) with depth.

denote the distance at which the caustics intersect the Earth's surface.

P waves interacting with the Earth's inner and outer core boundaries provide an example of both the waveform complexity induced by a discontinuous velocity increase and a discontinuous velocity decrease. A shadow zone and caustic are induced by a discontinuous velocity decrease at the core–mantle boundary, and a triplication is induced by a discontinuous velocity increase at the inner core boundary (**Figure 6**). The velocity decrease at the core–mantle boundary generates a reversal of the traveltime–distance curve and strong focusing of waves at the caustic distance B. The discontinuous increase in velocity at the outer core–inner core boundary generates the triplication C–D–F.

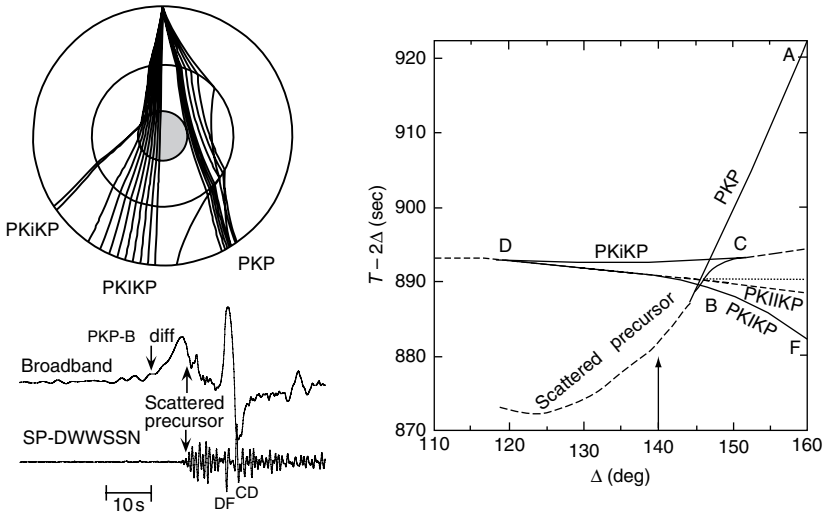

Figure 6 Rays and traveltime curves of P waves interacting with the Earth's inner and outer cores. Bottom left: Observed broadband displacement and narrow band-passed velocity (SP-DWWSSN) seismograms from a deep earthquake recorded near 140°.

Frequency-dependent diffraction occurs along the extension of BC to shorter distance. A lower-amplitude partial reflection along the dashed segment extends from D to shorter distances. In addition to the effects induced by radially symmetric structure, lateral heterogeneity near the core–mantle boundary can scatter body waves in all directions. The curved dashed line extended to shorter distances from point B in **Figure 6** represents the minimum arrival time of high-frequency energy scattered from either heterogeneity near or topography on the core–mantle boundary.

Changes in the curvature of traveltime curves for waves also induce changes in the shapes of the waves associated with each multipath. These waveform distortions can be understood from geometric spreading effects. In an inhomogeneous medium, geometric spreading R is proportional to the square root of the product of the principal radii of curvature of the wave front,

$$R \propto \sqrt{r_1 r_2} \qquad [9]$$

In a homogeneous medium, where wave fronts are spherical, $r_1 = r_2$, and geometric spreading reduces simply to the distance to the source. A wave front is described by a 3-D surface $\tau(\mathbf{x})$ over which traveltime is constant. Hence, the principal radii of curvature of the wave front are determined by the second spatial derivatives of the traveltime surface τ. From [9], a change in the sign of either of the two principal wave front curvatures (r_1 or r_2) produces a change in the sign of the argument of the square root in [9] and hence a $\pi/2$ phase change in the waveform associated with that wave front. A consequence of this relation is that any two waveforms having traveltime branches with a difference in the sign of the second derivative with respect to great circle distance, will differ by $\pi/2$ in phase. This $\pi/2$ phase change is called a Hilbert transform. A Hilbert transform of a delta function has a gradual positive onset, sharp downswing to negative values, and a gradual negative return to zero (**Figure 7**). The traveltime curve of the PKP waves along the AB branch in **Figure 6** has a concave upward curvature, while travel time curvatures of the PKP waves along the BC branch and the PKIKP waves along the DF branch are concave downward. Hence, waveforms of PKP-AB are Hilbert transformed with respect those of the PKP-BC and PKP-DF (**Figure 8**).

These changes in pulse shape are correct in the limit of infinite frequency, but at finite frequency pulse shapes near the cusps B, C, and D are neither delta-like nor Hilbert-transformed-like. Near these points, the shapes exhibit frequency dependence and appear as some kind of average of the two fundamental shapes. This type of pulse shape can also exist in cases where a reflection/transmission/conversion coefficient of a plane wave becomes complex, as in certain distance ranges of the SKS phase. In these cases, the pulse shape can be represented by a linear combination of a delta function and Hilbert-transformed delta function (Aki and Richards, 1980, pp. 157–158). In the shadows of cusps and caustics, diffracted waves exist, which decay with increasing frequency and increasing distance from the cusp or caustic (e.g., the diffracted PKP-B in the broadband seismogram in **Figure 6**).

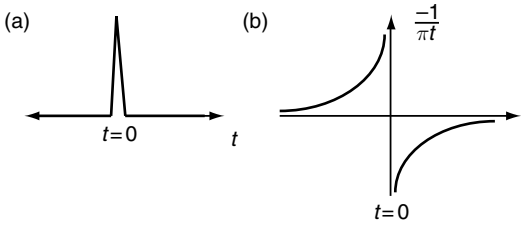

Figure 7 (a) Delta function and (b) its Hilbert transform.

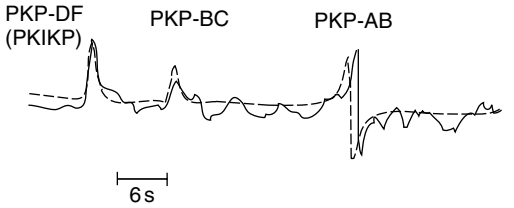

Figure 8 Observed and synthesized PKP waveforms from Choy and Cormier (1993). PKP-AB is Hilbert-transformed with respect to PKP-DF.

Waves having rays with multiple turning points also exhibit $\pi/2$ phase shifts for each turning point. Examples are PP waves and SS waves that are Hilbert-transformed with respect to the waveforms of the direct P and S waves, and waves multiply reflected along the underside of the core mantle boundary, such as PKKP, SKKS, PKnKP, SKnKS, etc. (Choy and Richards, 1975). In three-dimensionally varying media and for body waves having multiple turning points in waveguide-like structures, it is possible to have N multiple $\pi/2$ phase shifts for N turning points or N points of tangency to a caustic. N is termed the KMAH index (named after wave theorists Keller, Maslov, Arnold, and Hormander). The KMAH index is an important parameter to inventory

as rays are shot or traced in dynamic ray tracing (DRT). In DRT (Section 1.05.4.5), the KMAH index can be determined by tracking accumulated sign changes in the determinant of Cerveny's (2001) **Q** matrix, where geometric spreading R is proportional to the square root of the determinant of **Q**:

$$R \propto \sqrt{\det(\mathbf{Q})} \qquad [10]$$

In vertically varying, flat-layered models, $\det(\mathbf{Q})$ takes the form

$$\det(\mathbf{Q}) = \frac{\cos(i)}{V}\frac{\cos(i_o)}{V_o}\frac{X}{p}\frac{dX}{dp} \qquad [11a]$$

and in spherically symmetric Earth models,

$$\det(\mathbf{Q}) = (r\,r_o)^2\cos(i)\cos(i_o)\frac{\sin(\Delta)}{p}\frac{d\Delta}{dp} \qquad [11b]$$

In [11a] and [11b], vertical takeoff angle i, velocity V, and radius r having the subscript 'o' are evaluated at a ray origin or source point, and unsubscripted quantities are evaluated at a ray end point or receiver. X is the distance measured from source to receiver along the surface of the Earth model, and Δ is the great circle distance of the source to the receiver measured in radians. In [11a] the ray parameter p is that for rays in plane-layered models ($p = \sin(i)/V = \text{constant} = dT/dX$), but in [11b] p is that for rays in spherically layered models ($p = r\sin(i)/V = \text{constant} = dT/d\Delta$).

Head waves are another effect of a discontinuous velocity increase with depth that can induce frequency-dependent effects and waveform complexity. Head waves travel along the underside of a boundary in the higher-velocity medium. Depending on vertical gradient of the medium below the discontinuity, a head wave can either have an amplitude inversely proportional to frequency (no gradient) or be represented by an interference or a whispering gallery of waves multiply reflected along the underside of the discontinuity (e.g., Cerveny and Ravindra, 1971; Menke and Richards, 1980).

In some distance ranges, surface waves, and phases best described by modal representations interfere with body waves. Examples include late arriving body waves having multiple interactions with the core–mantle boundary and/or the free surface that interfere with fundamental mode Love and Rayleigh waves. Another example is shear-coupled PL waves that are generated by SV waves that turn in the mantle and excite converted P waves trapped in the crust (Baag and Langston, 1985). Shear-coupled PL waves can arrive as a dispersive wavetrain immediately following an SV wave in some distance ranges. The interference of shear-coupled PL waves with the direct SV phase has made it difficult to simultaneously model SH and SV phases to obtain mantle models from S waveforms (e.g., Helmberger and Engen, 1974). In this situation, it is important to choose an algorithm that includes a sufficiently complete set of rays or modes to represent both the direct body wave as well as the dispersed waves interacting with the crust and surface of the Earth.

1.05.3.2 Deep-Earth Structural Problems

The modeling problems of greatest research interest are structures in depth zones that introduce waveform complexity in the form of triplications, caustics, shadow zones, diffractions, head waves, and multipaths. For teleseismic observations, the zones of rapid spatial variation that are most often studied are the crust–mantle discontinuity (Moho), a regionally varying low-velocity zone in the upper mantle, narrow zones or discontinuities in velocity and density at or near 400 km, 500 km, and 660 km depth, a zone of regionally varying velocities between 100 and 300 km above the core–mantle boundary, and a 100–300 km region on both sides of the inner core boundary.

Key to the interpretation of these zones of rapid spatial variation is the relative changes in P velocity, S velocity, and density. From body-wave modeling, it is often only possible to make an estimate of velocity changes, either P or S velocity, but neither simultaneously, with little or no constraint on the associated density change. A common example of this is the estimate of the velocity increase required to reproduce the spacing of traveltime branches in the ranges of the triplicated portion of a traveltime curve due to a rapid increase in velocity with depth (e.g., **Figures 5** and **6**). The amplitudes of the body waves in the triplicated range, where one traveltime branch corresponds to a wave totally reflected from the discontinuity, have little or no sensitivity to any density change associated with the velocity change. The amplitude of a reflected body wave at more vertical incidence, however, is much more sensitive to the product of density and velocity changes (**Figure 9**). By combining observations of narrow angle and grazing incidence waves to a discontinuity, it is possible to remove or reduce the tradeoffs between velocity and density change. Combined

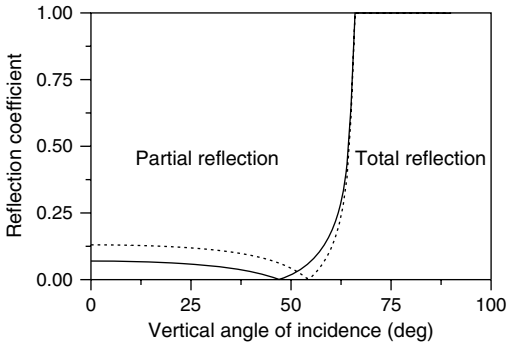

Figure 9 Example of a reflection coefficient showing total and partial reflection for a discontinuity for two cases: (1) velocity and density increase (solid) and (2) velocity increase identical but a different density increase (dashed). Note insensitivity of total reflection region to the size of the density increase.

modeling of P and S waveforms for both narrow- and wide-angle incidence then makes it possible to separately estimate P, S, and density changes at a discontinuity. From these estimates, it is possible to distinguish the nature of the discontinuity, for example, whether it is chemical change or a solid–solid mineral phase change.

When P- and S-wave waveform analyses are available, an additional diagnostic tool can be the calculation of the change in bulk sound velocity V_K, where

$$V_K^2 = V_p^2 - 4/3V_S^2 \qquad [12]$$

and V_P and V_S are the P and S velocities, respectively (Su and Dziewonski, 1997). Bulk sound velocities are more directly observed in high-pressure mineral physics experiments and theory, and can be directly compared against known mineralogy (Zhao and Anderson, 1994). Other constraints in interpreting 3-D variations in velocity are provided in comparing theoretical and observed estimates of the relative fractional changes in P velocity, S velocity, and density, $d\ln V_P/d\ln V_S$ and $d\ln V_S/d\ln \rho$ (e.g., Trampert *et al.*, 2001). Care, however, might be needed in comparing the frequency band of an observation with that of theoretical predictions due to the dispersive effects of viscoelasticity (Section 1.05.7.4; Karato, 1993).

The effect of temperature on velocity is known from experimental and theoretical predictions. Known temperature derivatives, or even practical bounds on the temperature derivative, can be used to determine whether a rapid velocity change is due to either a spatially sharp temperature, chemical, or phase change. In this analysis, it is also important to consider the effects of thermal diffusivity. For example, given an estimate of the thermal diffusivity, the spatial extent of a thermally induced velocity anomaly cannot persist at a scale smaller than a certain size. Thermally induced anomalies below this size diffuse away over time periods shorter than the timescale at which they are created by mantle circulation.

Estimating whether a region of velocity change is a true discontinuity or a transition spread out in space requires careful study of the frequency content of reflected and converted waves interacting with the region of rapid velocity change (*see* Chapter 1.17). This has been an enduring challenge in interpreting rapid changes in velocity in the upper mantle as solid–solid phase changes. Waves reflected at wavelengths much longer than the depth range of a gradient transition cannot distinguish a transition from a discontinuity. Shorter-wavelength waves, however, will not be reflected at narrow incidence angles. Reflected and converted waves at grazing incidence to a depth zone of rapid transition are relatively insensitive to the width of the transition even for a relatively broad frequency band of recording (e.g., Ward, 1978). Taking these sensitivities together, the frequency-dependent behavior of the amplitudes of body waves partially reflected at narrow angles of incidence to regions of rapid transition in depth can help diagnose whether a structure is a true discontinuity or transition zone. In practice, only a lower bound on the width of a depth transition can be safely diagnosed (e.g., Richards and Frasier, 1976), since there is typically an upper bound on the frequency (lower bound on wavelength) on observable teleseismic body waves (usually 2–3 Hz).

1.05.4 Modeling Algorithms and Codes

Modeling of body waves can be broadly classified into four approaches: (1) transform methods for spherically symmetric or plane-layered media, with some extensions for weak heterogeneity and anisotropy; (2) ray summation methods for regions in which frequency-independent ray theory is a good approximate solution; (3) mode summation methods; and (4) full or partial numerical solutions to elastic equations of motion that can treat the cases of strong heterogeneity, anisotropy, and small spatial scales of heterogeneity. A summary of these modeling methods follows. Published applications of each method are extensive,

and an attempt is made to primarily cite material in which the theory of each method is most completely developed. In many cases, this will be a textbook rather than a journal paper. Good starting points to obtain software for many approaches are the ORFEUS software library, codes deposited with the World Data Center as part of the *Seismological Algorithms* text, codes and tutorials by R. Hermann, example synthetics and codes distributed by the COSY Project, codes distributed on a CD supplied with the *International Handbook for Earthquake and Engineering Seismology* (Lee *et al.*, 2001), and computational seismology software available from the Computational Infrastructure in Geodynamics (CIG) web page.

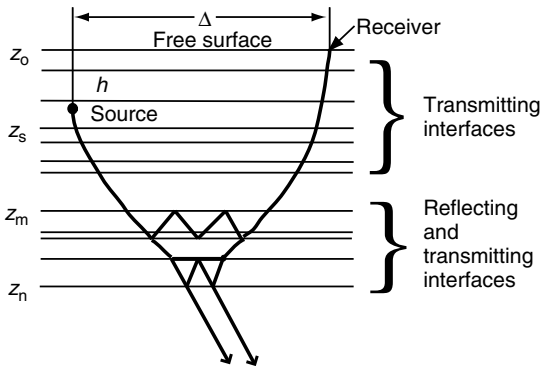

Figure 10 A typical layered model used in reflectivity synthesis, showing a transmission zone and rays reverberating in a reflection zone.

1.05.4.1 Reflectivity

Reflectivity (Fuchs and Müller, 1971; Müller, 1985; Kind, 1985; Kennett, 1983, 2001) is perhaps the most general and popular transform method of modeling seismograms in radially symmetric or plane-layered Earth models. Planar homogeneous layers parametrize the Earth model, after an Earth-flattening approximation (EFA) is applied. Plane-wave solutions of the wave equation are found in the frequency domain, with boundary conditions handled by propagator matrix techniques. This approach is used to derive a transformed solution at great circle distance Δ_o for displacement, $u(\omega, p, \Delta_o)$, in ray parameter and frequency space, where p is related to the horizontal component of the wavenumber vector by $k_z = \frac{\omega p}{r_e}$, with r_e the mean spherical radius of the Earth. The solution $U(t, \Delta_o)$ is then found by inverting Fourier transforms represented by

$$U(\omega, \Delta_o) = \frac{1}{2\pi} \int_{-\infty}^{\infty} d\omega e^{-i\omega t} \int_{\Gamma} dp\, u(\omega, p, \Delta_o) \quad [13]$$

Transform inversion is commonly accomplished by integrating $u(\omega, p, \Delta_o)$ along a contour Γ confined to a finite segment of the real p or k_x axis for the series of discrete 2^N frequencies required to invert the complex frequency spectrum by a fast Fourier transform (FFT).

Depending on the needs of the modeler, the integrand of [13] can be constructed to contain either one or several body-wave arrivals interacting with major discontinuities, fundamental or higher-mode surface waves, or a complete seismogram. In the most common applications, the integrand is constructed to represent the reflection of a body wave incident on a stack of layers in a reflection zone (**Figure 10**). Above the reflection zone, the incident wave is assumed to be transmitted down through and back up the layers overlying the reflection zone. Neglecting details of the source excitation, the factors making up $u(\omega, p, \Delta)$ include transmission coefficients T_D down and T_U up through the layers above the reflection zone, the reflection R_U from the reflection zone, and phase factor $\exp(i\omega p\Delta)$ accumulated through horizontal propagation to the great circle distance Δ, or

$$u(\omega, p, \Delta) \propto T_D R_U T_D \frac{\exp[i(\omega p\Delta - \pi/4)]}{\sqrt{\omega p \sin(\Delta)}} \quad [14]$$

The reflectivity response R_U can include all internal multiples and P-to-SV conversions within the thin homogeneous layers of the reflection zone. The reflectivity can be calculated from fundamental and propagator matrices. For example, R_U for SH waves can be calculated by solving the system

$$\mathbf{F}_o(z_1)\begin{pmatrix} 1 \\ R_U^o \end{pmatrix} = \mathbf{P}(z_1, z_N)\mathbf{F}_N(z_N)(T_D^N) \quad [15]$$

where R_U^o is the total wavefield reflected upward at the top of the boundary of the layered reflection zone and T_D^N is the total wavefield transmitted through the bottom of the reflection zone. A similar system can be set up for P and SV reflectivity, but care must be taken to rearrange the system to exploit algebraic cancellation of some exponentially growing terms for certain domains of ray parameter (Abo-Zena, 1979). Elimination of these troublesome terms can also be accomplished by rearranging the multiplication of fundamental matrices in such a way that also enables identification of infinite series of internal layer multiples. These interlayer multiples can be neglected after a small finite number of

reverberations (Kennett, 1983, 2001). Truncation of these internal multiples helps eliminate later-arriving energy that folds back into the finite time window required given by finite-length Fourier transforms. An alternative approach to eliminate the acausal arrival of the late-arriving interlayer multiples is to add a small imaginary part to each frequency $-i/\tau$ in the evaluation of the reflectivity response before inverting the Fourier transform (Kennett, 1979; Chapman, 2004, p. 361). Using the damping theorem of Fourier transforms, at each time point the inverted signal is then multiplied by the exponential $\exp(t/\tau)$.

After choosing a method to eliminate acausal late-arriving multiples, one must still decide on how to best suppress the numerical noise of the all of the causal internal layer multiples of the thin layers used to approximate a continuously varying model. This numerical noise can be minimized by either low-pass-filtering the response before inverting the Fourier transform or by making layer thicknesses smaller than 1/4 the shortest wavelength corresponding to the highest frequency of interest to model (**Figure 11**).

Parametrization of the spherical Earth by plane homogeneous layers with depth z first requires an EFA of velocities $v(r)$ of the type (Müller, 1977)

$$v_f(z) = \frac{r_e}{r} v(r) \qquad [16a]$$

$$z = r_e \ln\left(\frac{r}{r_e}\right) \qquad [16b]$$

Errors on the order of $1/\omega$ are introduced in synthetic seismograms in this process, and include problems associated with the decoupling of P and S wave potentials and the lack of an ideal density transformation (Chapman, 1973). The EFA will also breakdown at the center of the Earth ($r = 0$), limiting accurate modeling to body waves that penetrate only the upper 500 km of the inner core. With this limitation and unless applied to a region in which velocity gradients are anomalously high at very low (<0.01 Hz) frequencies, the EFA combined with thin homogeneous layering can usually be applied without introducing significant error in the modeling.

Another variant of the reflectivity method is the discrete wave number method, in which the integral over ray parameter p is replaced by a sum over discrete horizontal wave numbers, k_x (Bouchon and Aki, 1977; Bouchon, 1979). One advantage of this method is that it can include the zero wave number, which provides a solution for the static displacement near an earthquake source (Honda and Yomogida, 2003). The need for fictitious image sources to treat the surface boundary conditions introduces some complexity in the formulation of the discrete wave number method, but both SH and P-SV codes are available and well developed.

Because its input parameters are simple to understand, the reflectivity method is probably the most popular forward modeling technique. Input consists of an Earth model specified by velocities and densities in a stack of homogeneous layers, starting and

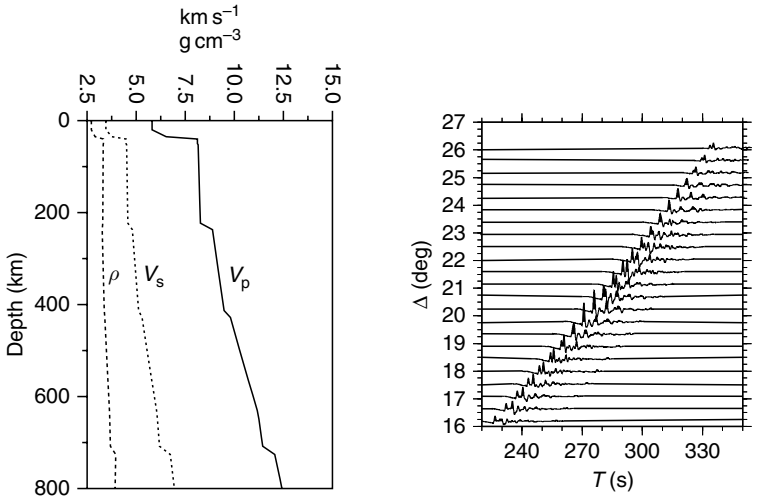

Figure 11 P waves synthesized by the reflectivity method using the program and example input provided by Kennett in the Orfeus web pages. Note the increase in amplitude around 20° associated with overlapping triplications induced by an upper-mantle model having rapid velocity increases near 400 and 700 km depth.

ending points of integration along a real ray parameter axis, a time window and sampling rate, and a simple source description. Some 2-D extensions are now available, allowing separate models to be specified in the source and receiver regions (see Section 1.05.7.1). Aside from simplicity of the input parameters, an advantage of reflectivity is that it easily allows the investigation of vertical transition zones in properties modeled by arbitrarily thin layers. This advantage, in common with all methods that allow for the insertion of thin layers, can lead to the neglect of physical constraints on radial derivatives of elastic moduli and density. Compared to ray-based methods that assume asymptotic approximations to vertical wave functions discussed in following sections, reflectivity can be numerically expensive for problems requiring thousands of thin layers.

1.05.4.2 Generalized Ray

The method commonly dubbed the generalized ray technique (GRT) originated from a technique of handling the integral transform inversions from ray parameter and frequency to time and space by the Cagniard–de Hoop method. It was recognized that most important teleseismic arrivals can be calculated by a first-motion approximation, allowing the time domain solution for ray interactions in each layer, both reflected and head waves, to be solved analytically (Helmberger 1974; Helmberger and Harkrider, 1978). Ray solutions within each layer are summed, usually just the first multiples. The volume of published applications using the GRT method is probably the largest of any other method, but its available computer codes are less widely circulated than those employing reflectivity methods. An application of GRT synthetics (Burdick and Helmberger, 1978) was instrumental in the first major revision of standard Earth models originating from the pioneering work of Jeffreys and Bullen, namely the replacement of a zone of strong velocity gradient in the upper mantle (Jeffreys, 1936) with two first-order discontinuities at 400 and 660 km depth (**Figure 12**).

The GRT commonly assumes an EFA and ignores higher than first-order internal multiples in each layer. It has been tested against other methods in many standard, vertically varying, Earth models and usually produces seismograms that are indistinguishable from those calculated by other common methods discussed in this chapter.

1.05.4.3 WKBJ-Maslov

A key difference in this technique is that thin homogeneous layers no longer parametrize the Earth model. Vertical gradients in depth or radius are allowed in velocity, and asymptotically approximate, WKBJ, solutions of the vertically separated part of the wave equation are assumed. In contrast to vertically homogeneous layers, where the up- and down-going vertical wave functions are simply $\exp[\pm ik_z(z-z_{ref})]$, the WKBJ solution approximates the vertical wave functions by

$$g^{(1)}_{(2)}(r, p, \omega) = \frac{e^{\pm i\pi/4}}{\omega r}\sqrt{\frac{V}{\xi(r)}}\exp(\pm i\omega\tau) \qquad [17a]$$

where the superscripts (1) and (2) refer to up- and down-going waves, respectively. $\xi(r)$is the vertical slowness and is related to the cosine of the angle of incidence of a ray at any level r by

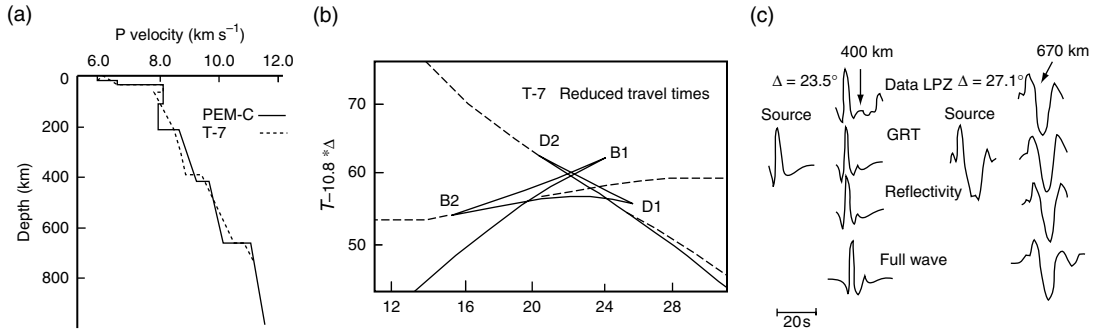

Figure 12 (a) Two models of P velocity in the upper 1000 km of the Earth. (b) Discontinuities at 400 and 650 km depth create two overlapping triplications in the traveltime curve and multiple phase arrivals in the great circle range 10–30°. (c) A comparison of observed and synthesized seismograms in the T-7 model for three different methods of synthesis that include diffraction effects (Burdick and Orcutt, 1978; Cormier and Choy, 1981).

$\xi(r) = \cos(i)/V = \sqrt{1/V^2 - p^2/r^2}$. τ is the delay time obtained by integrating the vertical slowness from the radius turning point radius r_p ,where $\cos(i) = 0$, to r:

$$\tau = \int_{r_p}^{r} \sqrt{1/V^2 - p^2/r^2} \qquad [17b]$$

The accuracy of these high-frequency approximations increases as the ratio λ/s decreases, where λ is the wavelength and s is the scale length of the medium. The scale length s is defined by

$$s = \min\left(\frac{V_S}{|\nabla V_S|}, \frac{V_P}{|\nabla V_p|}, \frac{\rho}{|\nabla \rho|}, r_b\right) \qquad [18]$$

where r_b is the radius of curvature of a first-order discontinuity in density or elastic velocity (Beydoun and Ben-Menahem, 1985). Separability of P and S wave potentials is assumed in each inhomogeneous layer, and frequency-dependent reflections and P-to-S conversions by regions of strong gradients are ignored. Hence, transition zones, which may be of interest to mantle solid–solid phase changes, should be handled by thin layers of weaker gradient where the asymptotic approximations remain valid. For problems consisting of a body wave reflected by or bottoming above a discontinuity, the integrand $u(\omega, p, \Delta_o)$ in [5] is replaced by

$$u(\omega, p) = \omega^{1/2}\Pi(p)e^{i\omega\theta(p)} \qquad [19a]$$

where

$$\theta(p) = \int_{r_p}^{r} \sqrt{1/v^2 - p^2/r^2} + \int_{r_p}^{r_o} \sqrt{1/v^2 - p^2/r^2} + p\Delta_o \qquad [19b]$$

$\Pi(p)$ is a product of the plane-wave reflection coefficient of the discontinuity and the plane-wave transmission coefficients through layers above the discontinuity. The factor $\theta(p)$ in the phase originates from the phases associated with the WKBJ solutions to vertical wave functions in the transmission region above the discontinuity and the horizontal wave function for propagation to great circle distance, Δ_o. Hence, the name WKBJ is applied to this method. In this method, body waves are synthesized by summing a series of representations of the type given by [19a]. Each body wave in this sum is assumed to be associated with rays that are either reflected by or turn just above the first inhomogeneous layer above each discontinuity (**Figure 13**).

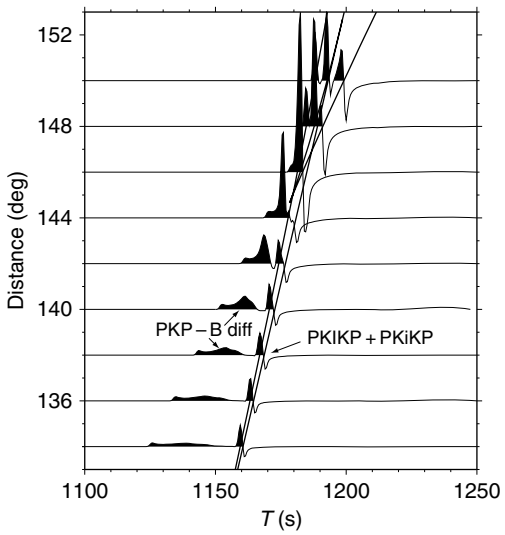

Figure 13 Seismograms synthesized by the WKBJ method for P waves interacting with the Earth's core using the program and example input by Chapman *et al*., (1988) distributed with *Seismological Algorithms*.

Inversion to the time and space domain of the transformed solution $u(\omega, p, \Delta_o)$ of [13] is performed by a slowness method rather than by a spectral method as commonly done in reflectivity methods. In slowness methods, the inversion to the time domain is performed analytically, recognizing that separate frequency-dependent factors in the integrand can be written as convolutions in the time domain. The final inversion to the space domain is performed by numerical integration over horizontal slowness p by a method in which the combined phase factor $\theta(p) - t$ is sampled in slowness intervals corresponding to a fixed sampling rate in time t (**Figure 14**). This key step is contained in the phase-sampling subroutine

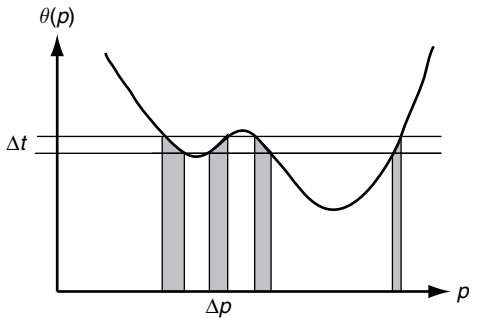

Figure 14 The ray parameter integrand in the WKBJ method is performed numerically by taking ray parameter intervals Δp equal to the desired sampling rate in time Δt as mapped by the total WKBJ phase function $\theta(p)$.

THETAC of Chapman's WKBJ original codes. The integration over horizontal slowness is truncated at points along the real p-axis, which introduces truncation phases in the synthetic. These can be removed by approximating the phase function's dependence on ray parameter from the truncation slownesses to ±infinity, assuming a linear dependence on p, and analytically integrating the approximation (Chapman, 1978). A well-documented package of the WKBJ algorithm by A.R. Gorman, tailored toward continental-scale reflection and refraction, exists in the PLOTSEC package. A code for teleseismic applications and example inputs can be obtained from Chapman's contribution to the *Seismological Algorithm* text. Software for the evaluation of the delay time $\tau(p)$ in many standard Earth models can be obtained from the TauP Toolkit (Crotwell *et al.*, 1999). Due to the need of separately describing ray interactions with discontinuities, the input to WKBJ codes is less black box-like than the input to typical reflectivity codes.

The Maslov technique (Chapman and Drummond, 1982) generalizes the WKBJ seismogram technique to 2- and 3-D velocity variations. The restrictions of the asymptotic approximations still apply, that is, the medium scale length in any inhomogeneous region must be greater than the wavelength. Full implementation of the technique sometimes requires an artful averaging of solutions in slowness p space with those in the physical x space. Each of these spaces can contain caustics where a weight factor or geometric spreading factor becomes singular. Regions of models having strong spatial gradients, where the asymptotic approximations are failing, are often characterized by closely spaced caustics in slowness space and physical space for waves at grazing incidence to the strong gradient regions. In these regions, the weight factors averaging the solutions in phase and physical space can be difficult to design. This situation can exist if high gradient zones define the boundaries of a thin high- or low-velocity zone (e.g., subducting slab or a fault zone). In these situations, it is better to define the anomalous structures by first-order discontinuities and apply boundary conditions for multiply reflected and refracted body waves.

Compared to the reflectivity method, the WKBJ and its related Maslov extensions are computationally much faster and, hence, better suited to problems in waveform inversion that may require many repeated syntheses to evaluate a misfit or object function. The speed of these methods is due to the use of an asymptotically approximate solution in spatially varying layers. Therein, however, lies the limitation of these methods. The vertical variation must be sufficiently weak so as not to exceed the errors associated with the approximation. When there is a need to sum ray interactions with more than two or three first-order discontinuities in a distance range, the input parameters describing the separate ray interactions in some WKBJ codes can become complex unless a user-friendly input interface is provided.

1.05.4.4 Full-Wave Theory and Integration in Complex *p* Plane

The term full-wave theory can be applied to any technique that incorporates frequency-dependent effects of wave interactions with boundaries, including diffraction and tunneling. Any transform approach that includes a broad enough domain in frequency and wave number to simulate these frequency-dependent effects, often due to poles or branch cuts in the response function, can be called a full-wave theory. This term was specifically applied by Cormier and Richards (1977) to an asymptotic spectral technique that inverts the slowness integral by paths Γ in the complex p plane and substitutes a Langer approximation for the WKBJ approximation to the vertical wave functions. The vertical wave function in the Langer approximation is given by

$$g^{(1)}_{(2)}(r, p, \omega) = \frac{\pi \rho_s V_s}{2\rho V} \frac{V_s e^{\pm i\pi/6}}{\omega \xi} \sqrt{\frac{\omega\tau}{V\xi}} H^{(1)}_{(2)1/3}(\omega\tau) \qquad [20]$$

The Langer approximation remains regular at grazing incidence to boundaries where ξ and τ vanish but returns the WKBJ approximation where it is accurate. The integration over the contour Γ is carried out numerically, with Γ extended into regions off the real p-axis where the integrand in [13] exponentially decays. For portions of Γ along the real p-axis, the integrand can be very oscillatory, and integration can be handled efficiently by Filon's method (Frazer and Gettrust, 1985). Full-wave theory includes tunneling, diffraction, and other phenomena related to frequency dependence of reflection–transmission coefficients at grazing incidence to boundaries. An example of the importance of these phenomena includes the very strong frequency dependence of the P wave that bottoms just above the core–mantle boundary and tunnels across the core–mantle boundary, exciting compressional (K) waves in the liquid outer core that multiply reflect along the underside of the core–mantle boundary

(PKnKP waves; e.g., Richards (1973). Applying attention to the validity of asymptotic approximations to the Legendre function representing the phase effects of propagating in the horizontal or Δ direction, full-wave theory has been extended to synthesize body waves that are strongly focused at the antipode by diffraction around spherical boundaries from all azimuths (Rial and Cormier, 1980).

The theory is most completely developed in chapter 9 of Aki and Richards (1981) and in *Seismological Algorithms* (Cormier and Richards, 1988), where example codes and inputs are distributed. As an asymptotic theory, full-wave theory shares the limitations of WKBJ codes, in that care must be taken not to assume too strong a velocity and density gradient in each inhomogeneous layer. Added to the complexity in the description of ray interactions shared with WKBJ code input, the construction of full-wave theory integrands and complex integration paths can be challenging, particularly for interference head wave and antipodal problems. Often it is best to start with example input files specifying ray descriptions and integration paths for these problems, which are distributed with *Seismological Algorithms*.

1.05.4.5 DRT and Gaussian Beams

DRT is simply a ray theory solution to the elastic equations of motion, consisting of a pulse arriving at the least or stationary phase time, scaled by the amplitude factors due to plane-wave reflection and transmission and geometric spreading. In an inhomogeneous region, DRT solutions in the frequency domain start from a trial solution in the form of factors multiplying inverse powers of radian frequency ω:

$$u(\omega) = \sum\nolimits_n \frac{A_n}{\omega^n} \exp(i\omega T) \qquad [21]$$

The errors in the approximation given by $n = 0$ remain small for wavelengths much smaller than the scale length of the medium given by [18]. In practice, no more than the $n = 0$ term is ever calculated, because higher-order terms are expensive to calculate and can never properly include the frequency-dependent effects of waves reflected and converted by regions of high spatial gradients in velocity and density. The review by Lambare and Virieux (this volume) provides further details on the derivation, accuracy, and frequency-dependent corrections to asymptotic ray theory and also reviews the relations between DRT, WKBJ/Maslov, and Gaussian beam summation.

Superposition of Gaussian beams is an extension of DRT and is closely related to the WKJB/Maslov techniques. It amounts to a superposition of approximated wave fronts, weighted by a Gaussian-shaped window in space centered about each ray. The shape of the wave front is estimated from the first and second spatial derivatives of the wave front at the end point of each ray. This is referred to as a paraxial (close to the axis of the ray) approximation of the wave front. To calculate the first- and second-order spatial derivatives of the wave front, a system of linear equations must be integrated. These equations, also required by DRT, consist of the kinematic equations that describe the evolution of ray trajectory, its vector slowness $\mathbf{p}$, and traveltime, an equation to describe the rotation of ray-centered coordinates in which S-wave polarization remains fixed, and a system of equations for matrices $\mathbf{P}$ and $\mathbf{Q}$ needed to describe the evolution of wave front curvature and geometric spreading. The vector slowness $\mathbf{p}$ is simply the spatial gradient of traveltime, and the geometric spreading is related to the wave front curvature or second spatial derivatives of traveltime. When a receiver is not near a caustic, the quantities determined from integrating the DRT system can be used to determine the frequency-dependent ray theory solution, consisting of geometric spreading, traveltime, and products of reflection/transmission coefficients. The paraxially estimated phase from the $\mathbf{P}$ and $\mathbf{Q}$ matrices of the DRT system can be used to either avoid two-point ray tracing by spatially extrapolating the traveltime near a ray or to iteratively solve the two-point ray-tracing problem. The traveltime at a point $\mathbf{x}$ in the vicinity of a ray end point at $\mathbf{x}_o$ can be estimated by:

$$T(\mathbf{x}) = T(\mathbf{x}_o) + \mathbf{p}\cdot\Delta\mathbf{x} + \frac{1}{2}\Delta\mathbf{x}^t\mathbf{H}^t\mathbf{M}\mathbf{H}\Delta\mathbf{x} \qquad [22]$$

where

$$\mathbf{M} = \mathbf{P}\mathbf{Q}^{-1} \text{ and}$$
$$\Delta\mathbf{x} = \mathbf{x} - \mathbf{x}_o$$

The 2×2 matrices $\mathbf{P}$ and $\mathbf{Q}$ are determined by integrating the systems

$$\frac{d\mathbf{P}}{ds} = \mathbf{V}\mathbf{Q}$$
$$\frac{d\mathbf{Q}}{ds} = v\mathbf{P} \qquad [23]$$

along the ray paths. In [22], $\mathbf{H}$ is the transformation between ray-centered coordinates to Cartesian

coordinates. The columns of **H** are the vector basis of the ray-centered coordinate system at the ray end point. **V** is a matrix of second spatial derivatives of velocity in the ray-centered coordinate system. The matrix **Q** can also be used to calculate geometric spreading [10]. The system in [23] can be generalized using a propagator, fundamental matrix formulism, similar to that used for propagating the solution to vertically separated equations of motion, except that in this system the solutions are quantities related to wave front curvature and ray density rather than components of displacement and stress.

Gaussian beams are defined by adding a small imaginary part to the matrix **M** in the paraxially extrapolated phase in [22], which gives an exponential decay of a beam in space away from the central ray. The amplitude of each beam is proportional to real part of $\exp(i\omega T)$, where T is made complex in [22] by the inclusion of a complex **M**. Beam summation remains regular in the vicinity of ray caustics, where geometric spreading vanishes and ray theory solutions become singular. It supplies estimates of frequency-dependent diffraction in the shadow of caustics and grazing incidence to boundaries.

To properly model classical head waves, some care must be used in the design of beam weighting and beam widths. Weight factors of beams are determined such that a superposition of beams returns a ray theory solution for the complex spectrum, that is, $U(\omega, x) = \exp(i\omega T)/\mathrm{sqrt}(\det(\mathbf{Q}))$, under a stationary phase approximation to an integral over ray parameter or take-off angles. Like the WKBJ/Maslov solution, Gaussian beams give a nonsingular approximation to the solution of the wavefield near a caustic. Restrictions on the validity of the method tend to be similar to that of the WKBJ/Maslov method. The scale length of the medium needs to be much larger than the wavelength and also larger than the beam widths (Ben-Menahem and Beydoun, 1985).

Compared to the Maslov technique, superposition of Gaussian beams has less mathematical support unless formulated in terms of complex rays as in some electromagnetic wave applications (Felsen, 1984). For grazing incidence to regions of strong velocity gradient, the paraxial approximation quickly fails and caustics become closely spaced, making it difficult to design optimal beam widths such that the paraxial approximation has small error in regions off the central ray where some beams may still have large amplitude.

The notational framework of the **P** and **Q** matrices and the propagator matrix of the dynamic ray-tracing system developed by Cerveny and his coworkers are powerful tools that can simplify the coding and understanding of any problem requiring the use of ray theory. The DRT notation can be exploited to calculate the integrand for Kirchhoff integrals and the banana-shaped kernels needed for frequency-dependent tomography.

Computer codes for superposition of Gaussian beams and DRT can be obtained from Cerveny's group at Charles University as well as the World Data Center. The best-developed codes are tailored to continental scale reflection–refraction problems. One version (ANRAY) is one of the rare codes that combines general anisotropy with 3-D variations. A teleseismic-oriented version of DRT and beam summation was written by Davis and Henson (1993), with a user-friendly graphical interface.

1.05.4.6 Modal Methods

Solutions of the elastic-wave equations can be obtained from either a superposition of ray/wave front solutions or from superposition modes (**Figure 15**). Rays and mode representations are fully equivalent in accuracy if properly applied to a specific Earth model and frequency domain. In a modal approach, the eigenfunctions of free oscillation of a sphere have a characteristic frequency, and are classified by the position of nodes at the surface and at depth where displacements go through a zero and change sign (e.g., Lapwood and Usami, 1981). For a modal solution to be accurate at the lowest frequencies of free oscillation, restoring forces due to gravity and rotation of the Earth must be included as additional forces in [1]. In a spherically symmetric, nonrotating, isotropic (SNREI) Earth, modes can be separated into either spheroidal or toroidal modes of oscillation. The motions of spheroidal modes are analogous to those of P and SV body waves and Rayleigh surface waves; those of toroidal modes to those of SH body waves and Love surface waves. Summation of normal modes of the Earth can provide a complete image of the wavefield at the surface and at every depth (Dahlen and Tromp, 1998). Every body wave observed at the surface can be represented by a subset of normal modes (**Figure 15**). The frequency-dependent effects of diffraction at ray-grazing incidence to boundaries are also included in mode sums. The normal modes of a SNREI Earth can be efficiently computed on a single processor for frequencies up to 0.1 Hz. A code by G. Masters for synthesizing seismograms from sums of normal mode

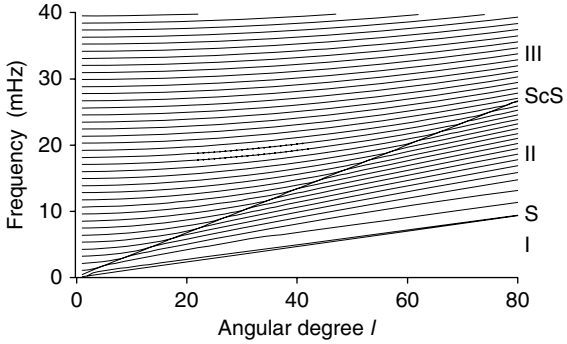

Figure 15 Torroidal modes in frequency and angular order number space, which, when summed, correspond to specific SH waves in the frequency and angular order number regions I, II, and III bounded by the two linear solid lines (Dahlen and Tromp, 1998).

is included on the CD supplied with the *International Handbook for Earthquake and Engineering Seismology* (Lee, *et al.*, 2001).

An advantage of mode summation is that input parameters are especially simple, basically just an Earth model parametrization, a frequency band, and desired number of modes. Mode summation is routinely used in the inversion of complete seismograms to retrieve moment-tensor representations of earthquake sources (Dziewonski *et al.*, 1981). A disadvantage is that it is limited to lower frequencies for practical computation on a single workstation. Effects of gravity, Earth rotation, anisotropy, and lateral heterogeneity remove degeneracy from SNREI modes and couple spheroidal with toroidal modes. Extensive literature exists on incorporation of the mode coupling induced by lateral heterogeneity by applying perturbation techniques to SNREI modes (e.g., Dahlen, 1987; Li and Tanimoto, 1993).

Another modal-type approach is that of locked modes (**Figure 16**). Here the modes are not whole-Earth modes of free oscillation, but rather the surface-wave modal energy that exponentially decays with increasing depth from the surface. Modes are numbered by sign changes in displacement with depth, the zeroth mode corresponding to either the fundamental mode Love or Rayleigh surface wave. The integrand $u(\omega, p)$ in [13] must first be constructed to include all interactions with the surface. The locked-mode approach then evaluates the ray parameter or wave number integral of [13] in the frequency domain by deforming the integration contour in the complex plane and applying the residue theorem to the integrand. A high-velocity capping layer is placed at depth, which locks plate-like modes into layers above the capping layer. The capping layer is placed deep enough such that mode sums representing waves of interest in a particular time window all turn or refract above the capping layer. Since all body waves, multiply reflected in the layers above the capping layer, are included, the locked-mode technique has a problem shared with the conventional reflectivity technique in which late-arriving waves are folded back into a finite-length time window. Similar to reflectivity, this problem can be handled by adding a small complex part to frequency. Harvey (1981) describes derivation of the technique in models described by plane homogeneous layers and available codes. An extension to vertically inhomogeneous layers using the Langer approximation is given by Cormier *et al.* (1991).

1.05.4.7 Numerical Methods

Fully numerical solutions of the elastic equations of motion can treat wave propagation in an arbitrarily complex 3-D Earth, having velocity variations over a broad range of scale lengths. A full solution is obtained, containing body waves, surface waves, and all diffraction, head-wave and leaky mode effects. Chapter 1.06 reviews numerical techniques, concentrating on current methods that can handle fully 3-D models and complete seismograms. This subsection is a brief summary of some of the techniques that occur in the expanded discussions in Chapter 1.06, including both 2-D and 3-D techniques and those that are applied to primarily the highest-frequency body waves and shorter time windows.

The principal numerical techniques are finite difference and finite element. For accuracy up to ranges

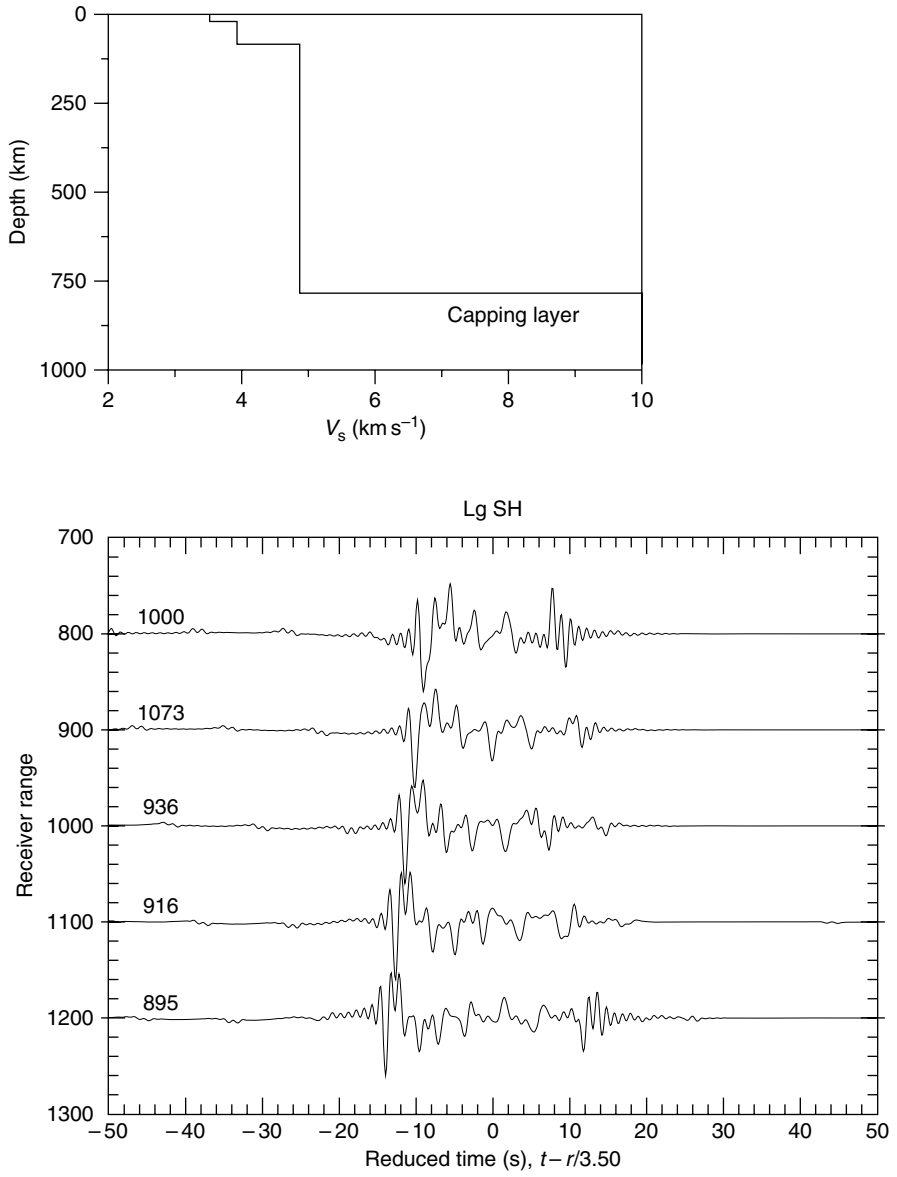

Figure 16 A crustal model and transverse component seismograms synthesized by the locked-mode method using programs by Harvey (1981). The Lg modes have a ray analog in multiple, Moho critically reflected, S waves reverberating in the Earth's crust. A high-velocity capping traps Love modes in the layers above the capping layers.

of 100 to 1000 wavelengths, conventional finite difference solutions typically are performed with fourth- to eighth-order difference approximations to spatial derivatives. The equations of motion are most commonly solved for particle velocity and stress on a staggered grid (Virieux, 1985, 1986). The pseudospectral method (e.g., **Figure 17**) calculates spatial derivatives in the wavenumber domain, multiplying by ik and inverse Fourier transforming back to space. It is computationally more expensive than higher-order differences but achieves much higher accuracy at long ranges, typically having little grid dispersion in applications to ranges of 10 000 wavelengths or higher. For this reason, the pseudospectral method can be an ideal choice for teleseismic applications, where high accuracy is desirable at both regional and teleseismic range. Kosloff and Kessler (1990) and Fornberg (1998) review both conventional finite difference and pseudospectral numerical approaches, estimating error and stability conditions.

The spectral element method (SEM) formulated with the SPECFEM code (Komatitsch and Vilotte,

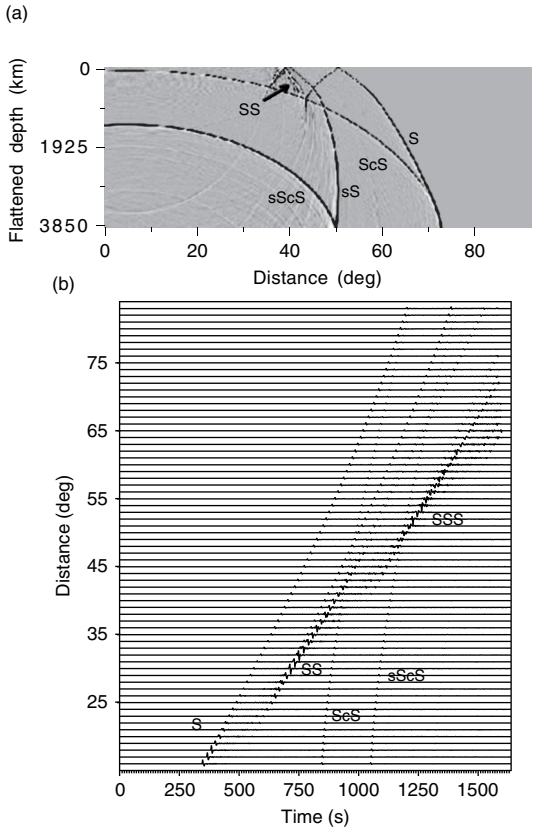

Figure 17 Wave fronts (a) and complete transverse (SH) component seismograms (b) synthesized by the pseudospectral method from Cormier (2000). Note the increase in amplitudes occurring at roughly 20° intervals in S, SS, and SSS due to rapid increases in velocity at upper-mantle solid–solid phase transitions.

1998; Komatitsch and Tromp, 1999, 2002) is currently one of the few numeric methods designed to handle a fully 3-D Earth model. SPECFEM has a well-developed interface to grid the elements needed for arbitrarily complex 3-D models. Versions of SPECFEM are available for both local/regional-scale problems for ranges on the order of 0–100 km, and for global- or teleseismic-scale problems. Another popular regional scale code is the elastic finite difference program by Larsen and Schultz (1995), which has been applied to the effects of 3-D basins and extended fault slip (e.g., Hartzell *et al.*, 1999).

The direct solution method (DSM) is a numerical technique that numerically solves the equations of motion for a series of frequencies required for inversion to the time domain by an FFT (Cummins *et al.*, 1994a, 1994b). The particular numerical technique consists in expanding displacements in the frequency domain by a series of basis functions consisting of a product of splines in the vertical direction and spherical harmonics in the angular direction. In some respects, the use of basis functions is similar to pseudospectral methods that represent the spatial spectrum of model variations by Fourier or spherical harmonic series. In DSM, the coefficients for the basis functions are found by the method of weighted residuals (Geller and Ohminato, 1994). The SH and P-SV seismograms be computed by DSM are complete, in that they contain all possible body and surface waves. Hence, DSM is a viable alternative to summing modes of free oscillation. Weak 3-D perturbations to a radially symmetric background model are possible in DSM at a computational cost not much higher than that required for the background model (Takeuchi *et al.*, 2000).

Computational time is a practical limitation to numerical modeling. Since most numerical techniques require Earth models specified on a spatial grid or elements, it is straightforward to parallelize the computation by decomposing the spatial grid or elements over multiple processors. Practical computations can be defined by time required to compute a problem. Depending on the algorithm and frequency band, common computer resources in most labs allow a complete teleseismic wavefield to be synthesized in 1 or 2 days using 10–100 processors in parallel. Typical body waves having a high signal-to-noise ratio in the teleseismic range (10–180°) exist up to 2 Hz. Practical 2-D modeling can be currently performed at teleseismic range up to 1 Hz with finite difference and pseudospectral methods; 3-D problems with the SPECFEM finite element method can be done up to 0.1 Hz in this time period with a similar number of processors. At ranges less than 100 km, 3-D problems can be practically performed at frequencies up to 1 or 2 Hz (order of 200 wavelengths). This range and frequency band just starts to cover the frequencies of interest to strong ground motion. Frequencies up to 10 Hz at 2000 km range (>5000 wavelengths) in complex 3-D structure are of interest to the problem of discriminating earthquake sources from underground nuclear tests. This is a research problem that is still inaccessible with small to moderate size clusters (less than 100 nodes) and numerical methods.

A large body of literature exists in the application of finite difference and pseudospectral solutions for local-scale problems up to 100 km for exploration applications and strong ground motion applications (e.g., Harzell *et al.*, 1999; Olsen, 2000) Significantly smaller amounts of published work exists for

applications at regional distances (100–2000 km), in which waves are primarily trapped in the crust and the uppermost mantle, and a much smaller amount exists for teleseismic propagation (e.g., Furumura *et al.*, 1998; Igel, 1999; Cormier, 2000).

1.05.5 Parametrization of the Earth Model

An important choice in modeling a seismogram will be the parametrization of the Earth model, or how to describe the spatial variation of its elastic moduli and density (**Figure 18**). The choice of parametrization can have important geodynamic and geochemical implications and is often tightly coupled to the choice made for the modeling algorithm (*see* Chapter 1.23).

1.05.5.1 Homogeneous Layers Separated by Curved or Tilted Boundaries

Certain parametrizations allow seismograms to be synthesized by simple analytic formulas. For example, if the Earth is isotropic and homogeneous, then ray paths are straight lines. The amplitude of body waves are inversely proportional to distance between source and receiver, $1/|\mathbf{x}_o - \mathbf{x}|$. A received waveform is simply the far-field approximation of the source–time function $S(t)$ evaluated at the retarded time, $S(t - |\mathbf{x}_o - \mathbf{x}/v|)$. This simple solution can be extended to models described by sequences of homogeneous layers bounded by planes of varying dip by incorporating elastic boundary conditions at each boundary to calculate reflection/transmission/conversion coefficients. Snell's law is applied in an

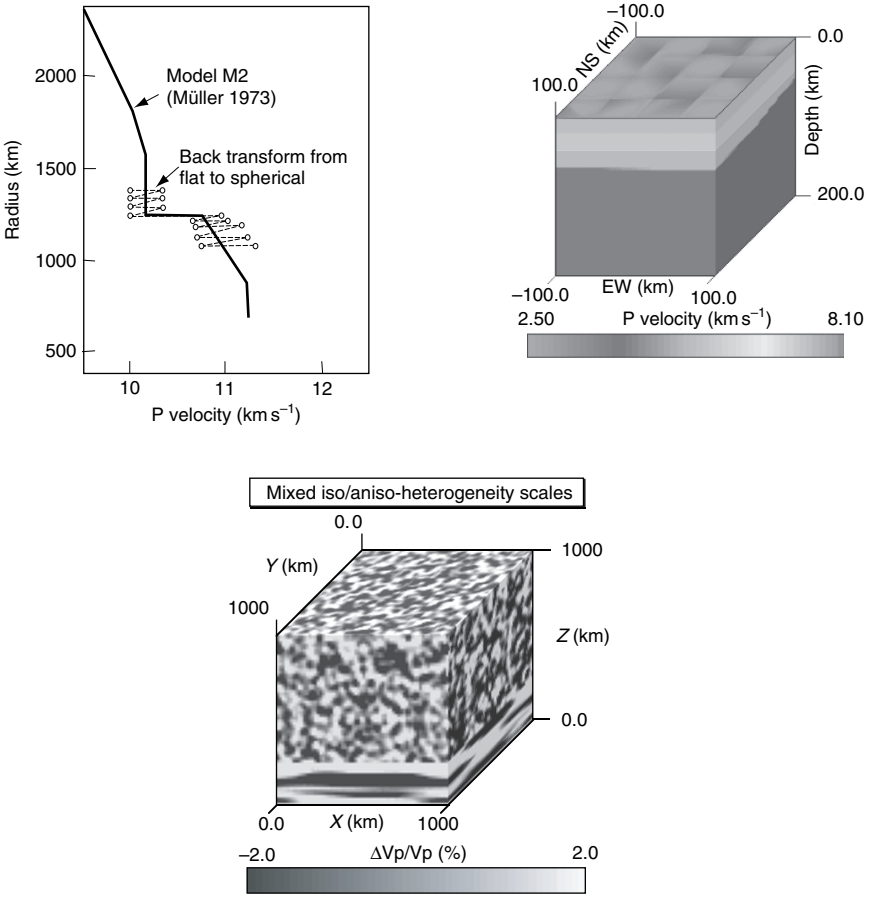

Figure 18 A comparison of the PREM model parametrized by continuous polynomials in radius vs the EFA and discrete homogeneous layers and discrete parametrization back-transformed to a spherical model (Müller, 1973; Aki and Richards, 1980). Bottom left: A 3-D model of the crust and uppermost mantle beneath Nilore, Pakistan, parametrized by Delaunay tetrahedra constructed from codes by Sambridge and Gudmundsson (1998). Bottom right: A 3-D model for testing the effects of possible structure near the core–mantle boundary having P velocity perturbations with both isotropic and anisotropic spatial distributions, constructed using the techniques described by Frankel and Clayton (1986).

incidence plane defined by ray direction and interface normal. Geometric spreading can be calculated from a simple function of ray length in each layer. This algorithm is just DRT applied to homogeneous layers.

Stacks of homogeneous layers can accurately describe continuous spatial variations, provided that the discretization of the model is much finer than the shortest wavelength of interest. The accuracy of the ray solution depends on the ratio of wavelength to boundary curvature. The frequency dependence of reflection by curved boundaries can be treated by the Kirchhoff integral technique.

1.05.5.2 Vertically Inhomogeneous Layers

Except for the case of back-of-the envelope calculations and the limiting case of layering much finer than wavelength, the Earth cannot often be well approximated by either homogenous planar or radially symmetric layers. Velocities and densities vary in all three coordinate directions, but the next most important approximation of the Earth is to make this variation occur in the vertical direction. If this vertical variation is approximated by thin homogeneous plane layers and an EFA (Section 1.05.4.1), then simple plane wave or analytic solutions to the wave equation can still be effectively employed in each layer. In addition to errors associated with the EFA, this discretization should consider physical constraints of finite-strain and buoyancy neutrality to be realistic, or at least the consequences of those constraints need to be evaluated. Except at near-vertical incidence, body waves are notoriously insensitive to density variations and it is especially easy to ignore unphysical effects of any constraints on the velocity–density relations of known materials or the geodynamic effects of buoyancy. The parametrization of the Earth by polynomials analytic in depth was proposed in Preliminary Reference Earth Model (PREM; Dziewonski and Anderson, 1981) in part to obey the constraints of stable stratification. Modifications to PREM and other reference earths should attempt to take similar care in obeying such constraints. Methods using asymptotic-ray approximations to vertical wave functions (e.g., WKBJ, full wave, GRT) are readily adaptable to this parametrization simply by extending the calculation of delay time $\tau(p)$ to numerical integration over radius or depth. Alternative parametrizations in radius ($V = ar^b$ and $V = a + br$) are computationally more efficient, but little penalty is involved with current-generation processors by calculating $\tau(p)$ by numerical integration over radius.

1.05.5.3 General 3-D Models

Tomographic models are often the starting point of synthetic modeling. The two most common parametrizations of these 3-D models are either by spherical harmonics (e.g., Gu *et al.*, 2001; Masters *et al.*, 2000; Ritsema and van Heijst, 2000; Chapter 1.10) or by block volumetric elements (e.g., Grand *et al.*, 1997). Except in fully 3-D modeling methods such as SPECFEM, a choice made in all 2-D modeling methods is to assume that body-wave propagation remains in the sagittal plane and to compute motions in a 2-D model derived by taking a cross section of the 3-D model. If velocity perturbations are assumed to be the same as the typically small (<3%) perturbations of the original tomographic model, the assumption of propagation remaining within or close to the sagittal plane is quite accurate. Indeed, to be consistent with the assumptions of linearized tomographic inversion, it is appropriate to even assume that paths are unperturbed from those in a reference model in the computation of traveltimes in ray-based methods. In this case, the results of the forward modeling can be disappointing, in that the only change in synthetic seismograms from those computed in a reference model will be small changes in relative traveltimes with little or no waveform perturbations. Larger variations in amplitudes and waveforms can be achieved with higher perturbations that violate the assumptions of linearized tomographic inversions.

Since tomographic imaging can smear a more intensely perturbed anomaly over its sampled ray paths into a smoother, less intense anomaly, one approach that has been used in forward waveform modeling is to multiply the perturbations of the tomographic starting model by a scale factor. Some success in matching waveforms by this technique has been achieved using factors of 2–3 to multiply the images of tomographically estimated perturbations to shear velocity (Ni *et al.*, 2000). Some adjustments in the boundaries of anomalies were also necessary to obtain good matches with observed waveforms. Starting with a tomographic model parametrized by spherical harmonics, Breger and Romanowicz (1998) and To *et al.* (2005) achieve a good match to S waves interacting with the core–mantle boundary by preserving the boundaries between the largest-scale positive and negative velocity anomalies but

increasing the maximum and minimum values of velocity perturbation.

A simple parametrization allowing for fast analytic computation of amplitudes and ray paths is that used by the code Raytrace3D by Menke (2005), which can be downloaded from the IRIS web site. The Earth model is parametrized by tetrahedra constructed from a grid specified in Cartesian coordinates. Linear interpolation of velocities between knots ($v = a + bx + cy + dz$) is assumed in each tetrahedral element, allowing ray paths to be computed analytically as summed segments of circles. Although geometric spreading is also analytically calculated, this code is primarily intended for calculating traveltimes rather than synthetic seismograms at local and regional ranges. The fast analytic computation of traveltimes and ray paths of this code are ideal for nonlinear tomographic inversions, where it is necessary to assume large perturbations from a background model.

Sophisticated and user-friendly tools for gridding 3-D models have existed in exploration and engineering applications for some time, but are often available only as expensive commercial packages. One public domain package is distributed with the finite element SPECFEM code. Another set of tools are those that employ irregular cells specified by Voronoi tetrahedra, which use a nearest neighbor interpolation to calculate velocities and their first spatial derivatives on irregularly spaced 3-D grids (Sambridge and Gudmundsson, 1998). This is can be used in conjunction with the convex hull grid mapping software from University of Minnesota to retrieve a physical quantity and its spatial derivatives at any coordinate point. One example where this approach can be examined are the 3-D slab models shown in Sambridge's web pages, where velocity perturbations have been centered on Benioff zone seismicity.

Some computational difficulties can arise in the parametrization of general 2-D and 3-D models due to the handling of first- and higher-order spatial derivatives of velocity. Ray and asymptotically approximate methods of solving elastic propagation are strictly valid for relatively slow spatial variation of velocity, where medium-scale lengths are much larger than wavelength. Some parametrizations that interpolate velocities in space can introduce high gradients in velocity that lead to false caustics where geometric spreading fails. Spatially continuous interpolations like spherical harmonics and cubic splines can introduce large first- and second-order spatial derivatives of velocity as perturbations increase. Some DRT codes use a spline-under-tension routine (Cline, 1974) to interpolate between velocities specified at grid points to reduce the size of spurious gradients introduced by the interpolation. In cases of high perturbations, the wave interactions with anomalies must be treated by solving boundary conditions on discrete scatterers (e.g., Korneev and Johnson, 1993; Imhof and Toksoz, 2001).

Rapid advances in computation have made it possible to more routinely include the effects of heterogeneity on the scale of wavelengths using numerical finite difference and finite element methods. It is usually impossible to deterministically know fine-scale structure except in a statistical sense as a spatial spectrum of heterogeneity. The most common way of constructing these types of models is to impose a random number generator at finite difference or element grid points, Fourier transform the grid from physical space to wavenumber space, filter by an assumed spatial spectrum of heterogeneity, and inverse Fourier transform to physical space (Frankel and Clayton, 1986). This idea has been extended to media that may be composed of 2 or n types of specific rocks or medium phases (Holliger *et al.*, 1993).

1.05.6 Instrument and Source

Assuming an Earth model and one of the algorithms previously described, a model response $M(t, \Delta_o)$ can be computed for a source consisting of a delta function in time and space. $M(t, \Delta_o)$ is termed the Green's function. The remaining task in synthesizing a body-wave seismogram consists in either incorporating or removing the effects of the seismograph response and source-time function. This task can be simplified using the ideas of superposition and linear systems. The seismogram can be thought of as a series of convolutions of a model response $M(t, \Delta_o)$, an instrument operator $I(t)$, a source time function $S(t)$, a receiver crustal response $C(t, \Delta_o)$, and an attenuation operator $A(t, \Delta_o)$:

$$U(t, \Delta_o) = I(t) * S(t) * C(t, \Delta_o) * A(t, \Delta_o) * M(t, \Delta_o) \quad [24]$$

The two common modeling choices to infer Earth structure are either to (1) convolve all of the operators in [24] and compare the resultant synthetic seismogram with an observed synthetic seismogram or to (2) deconvolve as many operators as possible to retrieve the model response. The first choice has

been the more common, but as the density of receiver and source arrays has approached that common in exploration seismology, the deconvolution choice has become increasingly popular. Deconvolution can increase the frequency content of the wavefield, and hence its spatial sensitivity. It allows different sources, receivers, and instruments to be combined to invert an observed wavefield to an image of reflectors and scatterers (e.g., Rost and Thomas, 2002).

1.05.6.1 Instrument Responses and Deconvolution

The Fourier transform of $I(t)$, or $I(\omega)$, is a filter that is a typically a narrow band pass of particle velocity. Most instrument responses are now reported by complex poles, ω_{p}^{i}, and complex zeros, ω_{o}^{i}, from which the complex frequency response $I(\omega)$ of the seismograph can be represented by

$$I(\omega) = \frac{(\omega-\omega_{\mathrm{o}}^{1})(\omega-\omega_{\mathrm{o}}^{2})\cdots(\omega-\omega_{\mathrm{o}}^{n})}{(\omega-\omega_{p}^{1})(\omega-\omega_{p}^{2})\cdots(\omega-\omega_{p}^{n})} \qquad [25]$$

The effect of the instrument can then be included by filtering the synthetic spectrum by multiplying by $I(\omega)$ and inverse Fourier transforming the result to the time domain. Alternatively, the instrument can be deconvolved by spectral division, but $I(\omega)$ must be modified by adding a constant term (water level) to avoid division by zero as the response goes to zero outside the pass band of the instrument. The instrument response can be deconvolved to displacement, velocity, or acceleration (**Figure 19**). The deconvolved particle velocity in the pass band of 0.01–2 Hz usually offers the best compromise between useful information content and high signal-to-noise ratio for teleseismic body waves. Deconvolved displacement, however, offers nearly a direct observation of the far-field source time function, given by shape of the P or S wave displacements in the range of 35–90°. In this range, the waveform of the observed displacement is primarily affected by the pulse broadening due to viscoelastic attenuation.

1.05.6.2 Far-Field Source Time Function

Detailed and accurate representation of the forcing function of the elastic equation of motion, or source-time function, requires the input of both theory and experiment for brittle failure and stick-slip friction. Chapter 4.02 provides a review of source representations and the physical assumptions behind them. For most modeling applications, a simple far-field representation and a judicious choice of earthquakes are all that is needed to begin to separate the effects of source from the effects of structure.

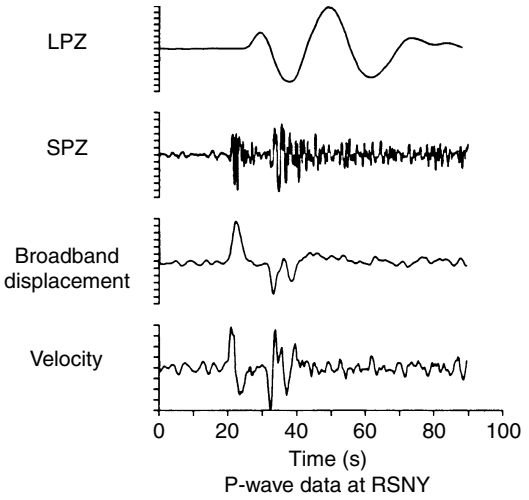

Figure 19 Instrument deconvolution showing a short- and long-period seismogram response and the deconvolved particle velocity and displacement from Choy and Engdahl (1987).

The far-field displacement is proportional to the time derivative of a moment-rate tensor $\mathrm{d}\mathbf{M}(t)/\mathrm{d}t$. A common scalar moment M_{o} can be factored out of $\mathrm{d}\mathbf{M}(t)/\mathrm{d}t$, leaving a far-field time source-time function $S(t)$. In the case of an earthquake faulting source, $S(t)$ is proportional to the time derivative of its slip history (e.g., Shearer, 1999, chapter 9). An operator combining the convolution of $S(t)$, $A(t, \Delta_{\mathrm{o}})$, and $C(t, \Delta_{\mathrm{o}})$ can be derived from either inversion or empirical observations of instrument-deconvolved P-wave displacements at all distances between 30° and 90°.

The $S(t)$ of many earthquakes having body-wave magnitudes less than 6.5 often can be adequately represented by a simple triangle-shaped pulse, where the triangle width is related to the corner frequency and fault length in a Brune (1970) model of the source spectrum. A body wave magnitude of 5.5 is often the practical lower limit to modeling, because earthquakes smaller than this size rarely generate sufficient teleseismic recordings of body waves having a high signal-to-noise ratio. After factoring out the time-dependent factor $S(t)$ and scalar moment M_{o} from the moment-rate tensor, a radiation pattern $R(\phi, p)$ can be constructed from weighted elements of the moment-rate tensor where ϕ is the azimuth and p is the ray parameter of a body wave ray

connecting source and receiver. This weighting is equivalent to representing general faulting by three fundamental types of faulting or source types (e.g., Aki and Richards, 1980, chapter 4).

The process of factoring out a slip-time history from a point-source radiation pattern should be avoided for earthquakes having body-wave magnitude greater than 6.5 or fault lengths greater than 50 km. For these larger earthquakes, a simple point-source representation fails, and the time history and the slip distribution become too complex to be easily separated from the waveform complexities due to structure.

If it were not for the fact that the majority of earthquakes are at depths of 20 km or less, incorporating a radiation factor $R(\phi, p)$ in the integrand of [13] would be all that is needed to include an earthquake source at teleseismic range. Since most earthquakes are shallow, the effects of surface reflections near the source (pP, sP) generally need to be included in modeling a 5–10 s time window surrounding an observed body wave. The effect of different radiation patterns for the near-source reflections is helpful in inversion of teleseismic P waves for the far-field moment-rate tensor (Langston and Helmberger, 1975). The inverted source depth and point-source representation (centroid moment-rate tensor) can be used to construct a predicted equivalent source-time function and radiation pattern containing P + pP + sP waves (**Figure 20**). Alternatively, the effect of the surface reflections can be handled by incorporating the moment-rate representation at the appropriate depth in reflectivity or mode summation techniques or be included by separately adding predicted pP and sP waveforms to P waveforms synthesized by ray-based or other transform methods.

At local and regional ranges, surface interactions as well as a more detailed source description can often still be handled by superposing far-field point-source representations. These point-source representations can be distributed at discrete points along fault plane, delayed by the time slip initiates and stops at each discrete point. This type of source representation is said to be kinematic rather than dynamic because the slip history is prescribed rather than resulting from a slip initiation condition related to either crack failure or friction on the fault surface. At very close range, the wavefield can be well approximated by a few simple directly arriving body waves, and the far-field Green's function for each body wave can be calculated by ray theory. The synthesis problem can then be reduced to an integral over the fault plane in which the integral is carried out over lines of equal arrival time of energy (isochrones) corresponding to the sum of the rupture time to a point on the fault and the traveltime of a body wave to a receiver (Spudich and Frazer, 1994). The effects of 3-D structure and frequency-dependent diffraction can be incorporated in this technique by substituting the ray-theoretical Green's functions with Green's functions calculated by Gaussian beam summation (e.g., Cerveny *et al.*, 1987) or WKBJ/

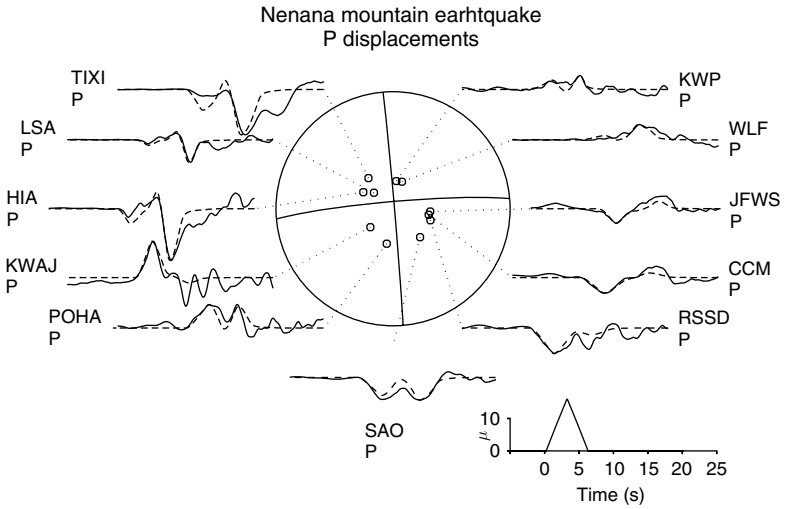

Figure 20 Teleseismic P-wave displacements for the Nenana earthquake of 23 October 2002. The broadband data are plotted as solid lines; the synthetic displacements are plotted as dashed lines. The far-field source-time function is plotted on the time axis, determined from modeling the P waves as a combination of P, pP, and sP waves (Choy and Boatwright, 2004).

Maslov superposition of plane waves. *See* Chapter 4.18 for a complete review of algorithms for synthesis at local ranges in which spatially extended slip models are required for earthquake slip inversions and simulation of strong ground motions.

1.05.7 Extensions

1.05.7.1 Adapting 1-D Codes to 2-D and 3-D

Since the delay time $\tau(p)$ in the WKBJ, GRT, and full-wave methods can be calculated from integrals of vertical slowness up to ray turning points, it is simple to consider different Earth models on either side of the turning points. For example, to calculate the effect of the upper mantle in the eastern US to a station in the western US, one might use two different models, keeping track of where rays enter and leave the two models (Helmberger *et al.*, 1996). In reflectivity methods, it is a little more difficult, but not impossible, to incorporate different receiver- and source-side models. One would need to separately consider a receiver- and source-side transmission response. Control of ray expansions within thin layers as in Kennett's formulation of the reflectivity method makes it possible to consider the effects of more general 2-D models.

Purely ray-based methods, such as DRT and/or superposition of Gaussian beams or Maslov plane waves, can consider continuously varying models in 2-D or 3-D space. Modal methods, including the locked-mode method, can be adapted to 2-D, 3-D, and anisotropic models by calculating the coupling between modes, including interactions between Love and Rayleigh modes. Maupin (1987), Maupin and Kennett (1989), and Kennett (1998) describe schemes for calculating modal coupling and show seismograms synthesized for rapid lateral transitions in crustal thickness.

1.05.7.2 Hybrid Methods

To save computation, it is sometimes necessary to combine two methods, a computationally cheaper method in a large region, and a computationally more expensive method in a small region to study structural complexity near a boundary or region of rapid velocity or density transition. Usually the computationally more expensive method is a numerical method, such as finite difference or spectral element. The usual way in which the two methods are connected is to compute a Kirchhoff integral. The integral is carried out on a surface or boundary that separates the structurally complex region from the simple region, employing Huygens principle to connect the wavefields in the two regions by allowing each point on a wave front to propagate as a new point source. Kirchhoff integrals can also be used to calculate the effects of scattering by inclusions or the frequency-dependent reflection or transmission across a curved interface when the radius of curvature is on the order of a wavelength. A hybrid method of this type was used by Wen *et al.* (1998) to study heterogeneity in the lowermost mantle using a finite difference method, connecting it to GRT in a radially symmetric overlying mantle. The most detailed treatment of fully elastic integrands for P, SV, and SH waves can be found in Frazer and Sen (1985). Probably due to the need for intense customization for specific problems, codes for Kirchhoff integrals are not generally distributed. A good starting point for any application are the acoustic problems described in Shearer (1999, pp. 138–140), which can then be generalized using the elastic formulas in Frazer and Sen (1985).

Capdeville *et al.* (2003a) developed a hybrid method that allows modal solutions in large homogeneous or weakly heterogeneous regions to be coupled to the numerical SEM solutions in strongly heterogeneous regions. This hybrid method has been applied to a thin, strongly heterogeneous, D″ region at the base of the mantle sandwiched between a homogeneous core and mantle (Capdeville *et al.*, 2003b; To *et al.*, 2005; *see* Chapter 1.18). A similar approach might also be feasible at higher frequencies and local and regional ranges by coupling locked surface-wave modes to SEM solutions.

1.05.7.3 Frequency-Dependent Ray Theory

Recognizing that ray theory is an approximation applicable at infinite frequency, corrections to ray theoretical approximation can be based on a Born approximation that corrects amplitude and traveltimes in such a way that a finite region in space determines the amplitude and traveltime of a body wave, making both depend on frequency (Dahlen *et al.* 2000). Chapter 1.04 provides a review and additional references on the calculation of these frequency-dependent corrections. One way in which the banana-doughnut sensitivity kernels needed to calculate the frequency dependence of traveltimes and amplitudes is to use the a paraxial approximation around a central ray using DRT. This approach can exploit the strong notational framework developed by Cerveny and colleagues

(e.g., Dahlen *et al.*, 2000). Sensitivity kernels derived from the Born approximation show that traveltime is most sensitive to velocity along the boundaries of the banana or rim of the doughnut away from the central ray, whereas amplitude is most sensitive to velocity in the center of the banana in the doughnut hole. The traveltime sensitivity is closely related to the behavior of the stationary-phase approximation, in which the path is assumed to be invariant for variations in velocity along the central ray. It is important to recognize that an accurate measurement of the frequency-dependent effects on traveltime depends on waveform measurements in which the effects on amplitude and phase are combined. To properly incorporate these combined effects in a tomographic inversion, a synthetic waveform must be cross-correlated with an observed waveform to obtain a traveltime residual. Except in tomographic inversion, these frequency-dependent corrections to ray theory using the Born approximation have not yet been used or tested as a general forward modeling technique. It is as yet unknown how the weak dispersion due to velocity variation tradeoffs with the weak dispersion due to viscoelasticity (Section 1.05.7.4), or how accurate the amplitude correction due to a simple Born approximation is compared to that predicted by the generalized Born approximation of Coates and Chapman (1991).

The frequency-dependent, banana-shaped, sensitivity kernels of seismic rays can also be calculated from a modal approach using a nonlinear perturbation theory (Li and Romanowicz, 1995). In this case, the forward modeling approach is mode summation. The approximations and behavior of errors due to asymptotic approximations of the effects of heterogeneous structure are better understood in this method but are practically limited to frequencies on the order of 0.1 Hz and lower.

1.05.7.4 Attenuation

Chapter 1.21 reviews the physical mechanisms and global models of seismic attenuation. Thus subsection reviews common procedures for incorporating attenuation into the synthesis of body waves.

Viscoelasticity is the term that best describes the type of seismic attenuation resulting from the dissipation of elastic energy into heat. This heat dissipation is analogous to the heat dissipated in electric circuits, where stress is analogous to current, voltage is analogous to strain, and complex impedance is analogous to a complex compliance (reciprocal of a complex elastic modulus). For ray-based and integral transform-based methods, viscoelastic attenuation is most directly treated by making velocity complex through the square root of a complex modulus divided by density. The effect of attenuation on the spectrum of a propagating body wave can be written as

$$A(\omega) = \mathrm{e}^{i\omega T(\omega)} \qquad [26]$$

where $A(\omega)$ is just the Fourier transform of the attenuation operator $A(t)$ in [24]. The complex traveltime $T(\omega)$ is determined by integrating a ray over a path in which velocity is complex and frequency dependent, or $T(\omega) = \int_{\text{path}} \mathrm{d}s/V(\omega)$.

The frequency dispersion of velocity in a viscoelastic medium is similar to the dispersion of a complex index of refraction in electromagnetic propagation, in which absorption is always associated with dispersion. In body waves, this dispersion is small and difficult to detect with narrow-band instrumentation. In sufficiently broadband recordings, viscoelastic dispersion is detectible as an asymmetry in the propagation of delta function time pulse. High frequencies travel faster than low frequencies, making a steeper rise time than fall time as the pulse propagates (**Figure 21**). Velocity dispersion was first recognized to be important in global seismology when the elastic moduli derived from the study of low-frequency free oscillations were found to be smaller than those derived from the traveltimes of high-frequency body waves (Dziewonski and Anderson, 1981).

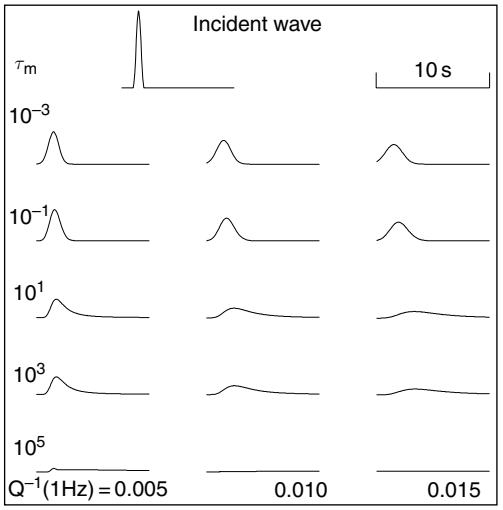

Figure 21 Attenuation operators convolved with a given wavelet for varying parameters of a viscoelastic relaxation spectrum from Li and Cormier (2002).

There is a consensus that the quality factor, Q, in the attenuation of teleseismic body waves is nearly independent of or slowly varying with frequency from 0.001 to 0.1 Hz, with possibly some stronger frequency dependence beginning between 0.1 and 1 Hz. For frequencies close to neither the low- or high-frequency corner of a relaxation spectrum (absorption band) of constant Q, this assumption leads to an approximate formula for complex velocity of the type

$$V(\omega) \cong V(\omega_r)\left(1 + \left(\frac{1}{\pi Q}\right)\ln\left(\frac{\omega}{\omega_r}\right) - i\left(\frac{1}{2Q}\right)\right) \quad [27]$$

where $V(\omega_r)$ is the real velocity at a reference frequency. Substitution of $V(\omega)$ into the ray path integral for complex time $T(\omega)$ in [26] and inverting the complex spectrum defines a time domain attenuation operator that is commonly termed the Futterman (1962) or Carpenter (1967) Q operator. This operator is valid in regions of the relaxation spectrum where attenuation $(1/Q)$ is constant. It is not valid near the corners of the true relaxation spectrum, where $1/Q$ decays as ω^{-1}. It is relatively simple, however, to derive a formula for complex velocity that is valid across the entire relaxation spectrum (e.g., Cormier and Richards, 1988). An example of the effect of attenuation operators constructed with this formula is shown in **Figure 21**.

The width of relaxation spectra in which attenuation $1/Q$ is nearly constant or slowly varying (often observed to be $\omega^{1/3}$) is typically 5 decades in frequency (Anderson and Given, 1981). A problem often not considered in modeling the effects of viscolasticity are the limitations viscoelastic theory imposes on the difference between the static (relaxed) elastic modulus and the infinite frequency (unrelaxed) modulus. There are limits on the band over which viscoleastic Q can be constant given by this modulus difference or defect. In practice, this means that any Q inferred from a body-wave pulse width or spectrum that has an exceptionally low value, for example, 10 or lower, is probably the result of scattering rather than viscoelasticity.

Slowness or ray-based methods often treat attenuation by solving the equations of motion with real velocities defined at the reference frequency (often chosen to be 1 Hz) and then convolving the result with the time domain attenuation operator of [26] appropriate for each ray path. Since the units of this ray-path integrand are time, a parameter often cited in the literature of teleseismic body waves is t^*. Considering only the real part of [26] and assuming [27] for $V(\omega)$, each frequency is exponentially attenuated by the factor $\exp(-\omega t^*)$, where

$$t^* = \int_{\text{path}} \frac{1}{V(\omega_r)Q}\,\mathrm{d}s \quad [28]$$

The parameter t^* is found to vary relatively slowly with range and path length of P waves in the mantle, and is on the order of 1 s for frequencies between 0.01 and 0.2 Hz in the distance range 30–90°.

Spectral methods that first compute the complex spectrum of the solution of the equation of motion (e.g., reflectivity, discrete wave number, full wave, the DSM , mode summation) can treat attenuation simply by substituting a complex velocity and analytically continuing all formulas in propagator matrices and phase factors that contain wave numbers and elastic moduli to complex numbers. To include the dispersive effect of attenuation in DRT and beam summation, a Futterman-type Q operator can be convolved with the computed amplitude of each ray or beam calculated in a model specified at a reference frequency. Another more general approach would be to compute amplitudes by DRT at the real velocities, $Re(V(\omega))$, defined at each frequency and then multiply each spectral component by an exponential scale factor

$$\exp\left(-\omega \int \mathrm{Im}\left(\frac{1}{V(\omega)}\right)\mathrm{d}s\right)^{-}$$

In finite difference methods that integrate the equation of motion in the time domain, it is not practical to handle viscoelastic attenuation by a convolution. Instead, it is possible to design a system of stress–strain memory functions that can be simultaneously integrated in the time domain with the equations of motion (Robertsson *et al.*, 1994). Using a memory function for only three specific relaxation times, it is usually possible to reproduce the effects of a relaxation spectrum of nearly constant attenuation in a frequency band of interest.

1.05.7.5 Anisotropy

Chapter 1.09 reviews the elastic anisotropy and computational approaches for its effects. Summarized here are considerations primarily related to ray- and transform-based methods of body-wave synthesis.

Elastic anisotropy removes the degeneracy of the S-wave eigenvalue/eigenvector solutions to the wave numbers of propagating plane waves. The SH

and SV definitions defined by source and receiver geometry are no longer useful for formulating boundary conditions needed for calculating reflection and refraction. S polarization is best resolved into components of motion along two orthogonal quasi-S-wave eigenvectors, with motion on both the SH and SV components of motion generally consisting of a combination of two quasi-S waves. A pure SV polarized wave incident on a weakly anisotropic region excites two transmitted quasi-S waves such that the SH component of the transmitted wave has the approximate shape of the time derivative of the SV component (Silver and Chan, 1991).

A special case of anisotropic propagation is that of transverse isotropy with a vertical axis of symmetry. In this case, the two-quasi S-waves are exactly polarized in the SH and SV directions defined by source–receiver geometry but with two different velocities. Transverse isotropy can be an accurate representation for Earth models consisting of thin planar or radially symmetric layers, having alternating or randomly fluctuation velocities and layer thicknesses much smaller than the smallest wavelength of interest (Backus, 1962). Transverse isotropy can be easily incorporated in all layered 1-D body-wave codes by modifying the calculations of reflection–transmission coefficients and the $\tau(p)$ function in the phase factor of WKBJ, GRT, or full-wave techniques (e.g., Chapman, 2004).

General anisotropy breaks the symmetry upon which some integral transforms and spherical harmonic analysis are based. Body waves can propagate in and out of the sagittal plane. This makes the problem of synthesizing body waves in a generally anisotropic model automatically a 3-D problem. In plane-layered models and Cartesian coordinates, the generalized wave number superposition leads to reflectivity formulations that require integration over two horizontal wave numbers to invert wave number transforms to the spatial domain (Fryer and Frazer, 1984, 1987). Similarly, the WKBJ/Maslov methods can be generalized by integrals over two horizontal slownesses (Garmany, 1989; Chapman, 2001). Some approximations for weak general anisotropy and expansion of the phase near its stationary point can be employed to simplify the problem to integration over a single wave number corresponding to waves propagating in and near the saggital plane. For seismograms synthesized by DRT or Gaussian beam summation, the kinematic system needed for ray trajectory and traveltimes is easily extended to the case of general anisotropy, where an eignevector–eigenvalue problem for the wave types is solved for each spatial or time increment used in numerical integration. A system for dynamic quantities corresponding to the **P** and **Q** matrices can be formulated for summation of Gaussian beams (Hanyga, 1986), but a more tractable approach is to take difference derivatives of ray positions and slownesses (Gajewski and Psencik, 1987) to determine geometric spreading and wave front curvature.

1.05.7.6 Scattering

Chapter 1.20 reviews seismic scattering. A few fundamental effects important to consider in the synthesis of body waves are reviewed here, some of which are computationally simple to include.

Single scattering by small-scale heterogeneity can be incorporated by a Born approximation (e.g., Chapman, 2004, chapter 10). The Born approximation effectively treats small perturbations in velocity and density from a background medium as seismic sources by moving terms due to the difference in perturbed velocity from the background velocity to the source side of the wave equation. The strength of these scattering sources that re-radiate energy are proportional to the energy of the wave incident on the heterogeneity and the size of its perturbations. For wavelengths much greater than the heterogeneity, each heterogeneity can be treated by a point-source representation similar to the moment-rate tensor representation of earthquake sources (Wu and Aki, 1985). The effects of many small-scale heterogeneities can be obtained by summing the radiated body waves of each small scatterer. The Green's function solutions of the equations of motion must be known from the source to the position of each scatterer and from the scatterer to the receiver. These Green's functions can be calculated by any of the methods described in Section 1.05.4. The volume of the region of scatterers contributing to a specific time window surrounding a body wave is the banana-shaped region surrounding a least-time ray described in Section 1.05.7.3. An example of this approach is the synthesis of the precursor coda of PKIKP from scatterers near the core–mantle boundary (Cormier, 1999).

Forward scattering in the direction close to the direction of the least-time ray can affect the pulse shape of broadband body waves. A finite frequency band of observation can blur the effects of many scatterers, whose arrivals can occur over time spacings much shorter than the shortest period in the

pass band of observation. This broadening and multipathing can be mistaken for the effects of viscoelastic attenuation. Unlike viscoelastic attenuation, where energy is lost to heat, scattering attenuation simply redistributes high-frequency energy in time and space out of a finite time window surrounding the pulse observed at a particular location. One recent approximate method of including this effect is the theory of dynamic composite elastic moduli (DYCEM) of Kaelin and Johnson (1998). This technique can be formulated in terms of a complex wave number, allowing it to be treated in much the same way as complex velocities in viscoelasticity (e.g., Cormier and Li, 2002).

1.05.8 Conclusions

Most of the algorithms for synthesizing body waves in radially symmetric (1-D) structure have been successfully tested and verified against each other (e.g., Choy *et al.*, 1980; **Figure 12**). Factors to consider in choosing an algorithm include the accuracy in a required frequency band and distance range, the width of the time window and number and types of seismic phases, speed of computation, the completeness of documentation, and the existence and accessibility of software.

The frequency band of calculation is probably the foremost important factor. If working in the frequency band less than several one-tenths of a hertz, then modal summation or the DSM are good choices because they easily include all possible body waves, surface waves, and frequency-dependent interactions with discontinuities in an arbitrarily wide time window at an acceptable computational cost on a single workstation. Using a perturbation approach, they can also handle weak lateral heterogeneity (several percent perturbation in velocity and density) with little additional computational overhead. At higher frequencies, reflectivity/GRT or locked-mode approaches in thin homogeneous layers or asymptotically approximate ray-based methods (WKBJ/full wave/Maslov/DRT and Gaussian beams) in homogeneous layers are efficient and produce identical results if carefully used.

In either low- or high-frequency bands, the most important limitations of each algorithm are related to its accurate reproduction of the waveform effects of the broad spatial spectrum of Earth structure. In all algorithms, it is important to consider the effects of neglecting small-scale structure on the order of a wavelength or smaller. In high-frequency algorithms, limitations are related to either the validity of the EFA, the physicality of thin-layer representations, or the validity of asymptotic approximations of wave functions in layers having continuous and large spatial gradients. Understanding these limitations is also key to the problems of separating the effects of anisotropy from heterogeneity and viscoelasticity from scattering.

Computational hardware now makes it possible to routinely model seismic waveforms to invert for both radially symmetric (1-D) Earth structure and simple point-source representations of earthquake faulting. Recent advances in digital recording and network telemetry have now made these inversions possible in near real-time. The remaining advance needed to fully exploit the real-time capabilities of 1-D modeling lies in making user-friendly software interfaces.

Three-dimensional modeling is still strongly limited by current computational hardware. Ray-based 3-D modeling is feasible on single workstations in smooth models having a relatively large ratio of scale length of heterogeneity to wavelength and for relatively mild velocity and density perturbations (less than several percent). Similarly, perturbation approaches based on mode summation or the DSM can be performed with modest computational overhead for relatively weak velocity perturbations (several percent) and at large scale lengths (thousands of kilometers). Investigation of effects of very small-scale heterogeneity (10 km or less) at high frequencies (>1 Hz) can be done in 3-D but is currently only practical for ranges on the order of hundreds of wavelengths using clusters of processors. An effort to test and verify 3-D modeling algorithms against each other has just begun in the last several years (Igel *et al.*, 2000).

Acknowledgments

The author thanks the National Science Foundation for continued support on problem in wave propagation and Earth structure, most recently under grant EAR 02-29586.

References

Abo-Zena A (1979) Dispersion function computations for unlimited frequency values. *Geophysical Journal of the Royal Astronomical Society* 58: 91–105.

Aki K and Richards PG (1980) *Quantitative Seismology: Theory and Methods*. San Francisco, CA: W.H. Freeman.
Aki K and Richards PG (2002) *Quantitative Seismology*, 2nd edn. Sausalito, CA: University Science Books.
Anderson DL and Given JW (1982) Absorption band Q model for the Earth. *Journal of Geophysical Research* 87: 3893–3904.
Baag C and Langston CA (1985) Shear-coupled PL. *Geophysical Journal of the Royal Astronomical Society* 80: 363–385.
Backus GE (1962) Long-wave elastic anisotropy produced by horizontal layering. *Journal of Geophysical Research* 67: 4427–4440.
Ben-Menahem A and Beydoun WB (1985) Range of validity of seismic ray and beam methods in general inhomogeneous media, Part I: General theory. *Geophysical Journal of the Royal Astronomical Society* 82: 207–234.
Bouchon M and Aki K (1977) Discrete wave-number representation of seismic wave source fields. *Bulletin of the Seismological Society of America* 67: 259–277.
Bouchon M (1979) Discrete wave number representation of elastic wave fields in three-space dimensions. *Journal of Geophysical Research* 84: 3609–3614.
Bréger L and Romanowicz B (1998) Three dimensional structure at the base of the mantle beneath the central Pacific. *Science* 382: 244–248.
Brune JN (1970) Tectonic stress and the spectra of seismic shear waves from earthquakes. *Journal of Geophysical Research* 75: 4997–5009.
Bullen KE and Bolt BA (1985) *Introduction to the Theory of Seismology*, pp. 499. Cambridge, UK: Cambridge University Press.
Burdick LJ and Helmberger DV (1978) The upper mantle P velocity stucture of the Western United States. *Journal of Geophysical Research* 83: 1699–1712.
Burdick LJ and Orcutt JA (1979) A comparison of the generalized ray and reflectivity methods of waveform synthesis. *Geophysical Journal of the Royal Astronomical Society* 58: 261–278.
Capdeville Y, Chaljub E, Vilotte JP, and Montagner JP (2003a) Coupling the spectral element method with a modal solution for elastic wave propagation in global Earth models. *Geophysical Journal International* 153: 34–66.
Capdeville Y, Romanowicz B, and To A (2003b) Coupling spectral elements and modes in a spherical Earth: An extension to the 'sandwich' case. *Geophysical Journal International* 154: 44–57.
Carpenter EW (1967) Teleseismic signal calculated for underground, underwater, and atmospheric explosions. *Geophysics* 32: 17–32.
Cerveny V and Ravindra R (1971) *Theory of Seismic Head Waves*. Toronto, ON: University of Toronto Press.
Cerveny V (1985) The application of ray tracing to the numerical modelin of the seismic wave field in complex structures. In: Helbig K and Treitel S (eds.) *Seismic Shear Waves: Handbook of Geophysical Exploration, Section I: Seismic Exploration*, vol. 15A, pp. 1–124. London: Geophysical Press.
Cerveny V, Pleinerová J, Klimes L, and Psencík I (1987) High frequency radiation from earthquake sources in laterally varying structures. *Geophysical Journal of the Royal Astronomical Society* 88: 43–80.
Cerveny V (2001) *Seismic Ray Theory*. New York: Cambridge University Press.
Chapman CH (1973) The Earth flattening transformation in body wave theory. *Geophysical Journal of the Royal Astronomical Society* 35: 55–70.
Chapman CH (1978) A new method for computing synthetic seismograms. *Geophysical Journal of the Royal Astronomical Society* 54: 481–518.
Chapman CH and Drummond R (1982) Body-wave seismograms in inhomogeneous media using Maslov asymptotic theory. *Bulletin of the Seismological Society of America* 72: S277–S317.
Chapman CH, Chu J-Y, and Lyness DG (1988) The WKBJ seismogram algorithm. In: Doornbos DJ (ed.) *Seismological Algorithms*, pp. 47–74. London: Academic Press.
Chapman CH (2004) *Fundamentals of Seismic Wave Propagation*. Cambridge, UK: Cambridge University Press.
Choy GL and Richards PG (1975) Pulse distortion and Hilbert transformation in multiply reflected and refracted body waves. *Bulletin of the Seismological Society of America* 65: 55–70.
Choy GL, Cormier VF, Kind R, Müller G, and Richards PG (1980) A comparison of synthetic seismograms of phases generated by the full wave theory and by the reflectivity method. *Geophysical Journal of the Royal Astronomical Society* 61: 21–39.
Choy GL and Cormier VF (1983) The structure of the inner core inferred from short-period and broad-band GDSN data. *Geophysical Journal of the Royal Astronomical Society* 72: 1–21.
Choy GL and Engdahl ER (1987) Analysis of broadband seismograms from selected IASPEI events. *Physics of Earth and Planetary Interiors* 447: 80–92.
Choy GL and Boatwright J (2004) Radiated energy and the rupture process of the Denali Fault earthquake sequence of 2002 from broadband teleseismic body waves. *Bulletin of the Seismological Society of America* 94: S269–S277.
Cline AK (1874) Six subprograms for curve fitting using splines under tension. *Communications of the ACM* 17: 220–223.
Coates RT and Chapman CH (1991) Generalized Born scattering of elastic waves in 3D media. *Geophysical Journal International* 107: 231–263.
Cormier VF (1999) Anisotropy of heterogeneity scale lenths in the lowermost mantle from PKIKP precursors. *Geophysical Journal International* 136: 373–384.
Cormier VF (2000) D'' as a transition in the heterogeneity spectrum of the lowermost mantle. *Journal of Geohysical Research* 105: 16193–16205.
Cormier VF and Choy GL (1981) Theoretical body wave interactions with upper mantle structure. *Journal of Geophysical Research* 86: 1673–1678.
Cormier VF and Li X (2002) Frequency dependent attenuation in the inner core: Part II. A scattering and fabric interpretation. *Journal of Geophysical Research* 107(B12): 2362 (doi:10.1029/2002JB1796).
Cormier VF, Mandal B, and Harvey D (1991) Incorporation of velocity gradients in the synthesis of complete seismograms by the locked mode method. *Bulletin of the Seismological Society of America* 81: 897–930.
Cormier VF and Richards PG (1977) Full wave theory applied to a discontinuous velocity increase: The inner core boundary. *Journal of Geophysics* 43: 3–31.
Cormier VF and Richards PG (1988) Spectral synthesis of body waves in Earth models specified by vertically varying layers. In: Doornbos D (ed.) *Seismological Algorithms*, pp. 3–45. London: Academic Press.
Crotwell HP, Owens TJ, and Ritsema J (1999) The TauP Toolkit: Flexible seismic travel-time and raypath utilities. *Seismological Research Letters* 70: 154–170.
Cummins PR, Geller RJ, Hatori T, and Takeuchi N (1994a) DSM complete synthetic seismograms: SH, spherically symmetric, case. *Geophysical Research Letters* 21: 533–536.
Cummins PR, Geller RJ, and Takeuchi N (1994b) DSM complete synthetic seismograms: P-SV, spherically symmetric, case. *Geophysical Research Letters* 21: 1663–1666.

Dahlen FA (1987) Multiplet coupling and the calculation of synthetic long-period seismograms. *Geophysical Journal of the Royal Astronomical Society* 91: 241–254.

Dahlen FA and Tromp J (1998) *Theoretical Global Seismology*, P. 944. Princeton, NJ: Princeton University.

Dahlen FA, Hung S-H, and Nolet G (2000) Frechet kernels for finite-frequency traveltimes-I. Theory. *Geophysical Journal International* 141: 157–174.

Davis JP and Henson IH (1993) Users Guide to Xgbm: An X-Windows System to Compute Gaussian Beam Synthetic Seismograms, Rept TGAL-93-02. Alexandria, VA: Teledyne-Geotech.

Doornbos DJ (*ed.*) (1988) *Seismological Algorithms: Computational Methods and Computer Programs*, P. 469. New York: Academic Press.

Dziewonski AM, Chou T-A, and Woodhouse JH (1981) Determination of earthquake source parameters from waveform data for studies of global and regional seismicity. *Journal of Geophysical Research* 86: 2825–2852.

Dziewonski AM and Anderson DL (1981) Prelminary reference Earth model. *Physics of the Earth and Planetary Interiors* 25: 297–356.

Felsen LB (1984) Geometrical theory of diffraction, evanescent waves, complex rays and Gaussian beams. *Geophysical Journal of the Royal Astronomical Society* 79: 77–88.

Fornberg B (1998) *A Practical Guide to Pseudospectral Methods*. Cambridge, UK: Cambridge University Press.

Frankel A and Clayton RW (1986) Finite-difference simulations of seismic scattering: Implications for the propagation of short-period seismic waves in the crust and models of crustal heterogeneity. *Journal of Geophysical Research* 91: 6465–6489.

Frazer LN and Gettrust JF (1984) On a generalization of Filon's method and the computation of the oscillatory integrals of seismology. *Geophsical Journal of the Royal Astronomical Society* 76: 461–481.

Frazer LN and Sen M (1985) Kirchhoff–Helmholtz reflection seismograms in a laterally variable multi-layered elastic medium. Part I. Theory. *Geophysical Journal of the Royal Astronomical Society* 80: 121–147.

Fryer GJ and Frazer LN (1984) Seismic waves in stratified anisotropic media. *Geophysical Journal of the Royal Astronomical Society* 78: 691–710.

Fryer GJ and Frazer LN (1987) Seismic waves in stratified anisotropic media – II. Elastodynamic eigensolutions for some anisotropic systems. *Geophysical Journal of the Royal Astronomical Society* 91: 73–101.

Fuchs K and Müller G (1971) Computation of synthetic seismograms with the reflectivity method and comparison with observations. *Geophysical Journal of the Royal Astronomical Society* 23(4): 417–433.

Furumura T, Kennett BLN, and Furumura M (1998) Seismic wavefield calculation for laterally heterogeneous spherical Earth models using the pseudospectral method. *Geophysical Journal International* 135: 845–860.

Futterman WI (1962) Dispersive body waves. *Journal of Geophysical Research* 67: 5279–5291.

Gajewski D and Psencik I (1987) Computation of high-frequency seismic wavefields in 3-D laterally inhomogeneous anisotropic media. *Geophysical Journal of the Royal Asronomical Society* 91: 383–411.

Garmany J (1989) A student's graden of anisotropy. *Annual Review of Earth and Planetary Sciences* 17: 285–308.

Geller RJ and Ohminato T (1994) Computation of synthetic seismograms and their partial derivatives for heterogeneous media with arbitrary natural boundary conditions using the direct solution method (DSM). *Geophysical Journal International* 116: 421–446.

Gilbert F and Backus GE (1966) Propagator matrices in elastic wave and vibration problems. *Geophysics* 31: 326–332.

Grand SP, van der Hilst RD, and Widiyantoro S (1997) Global seismic tomography; a snapshot of convection in the Earth. *GSA Today* 7: 1–7.

Gu YJ, Dziewonski AM, Su W-J, and Ekström G (2001) Models of the mantle shear velocity and discontinuities in the pattern of lateral heterogeneities. *Journal of Geophysical Research* 106: 11169–11199.

Hanyga H (1986) Gaussian beams in anisotropic elastic media. *Geophysical Journal of the Royal Astronomical Society* 85: 473–503.

Harvey DJ (1981) Seismogram synthesis using normal mode superposition: The locked mode approximation. *Geophysical Journal of the Royal Astronomical Society* 66: 37–69.

Harvey D and Choy GL (1982) Broadband deconvolution of GDSN data. *Geophysical Journal of the Royal Astronomical Society* 69: 659–668.

Hartzell S, Harmsen S, Frankel A, and Larsen S (1999) Calculation of broadband time histories of ground motion: Comparison of methods and validation using strong-ground motion from the 1994 Northridge earthquake. *Bulletin of the Seismological Society of America* 89: 1484–1504.

Helmberger DV (1974) Generalized ray theory for shear dislocations. *Bulletin of the Seismological Society of America* 64: 45–64.

Helmberger DV and Engen, GR (1974) Upper mantle shear structure. *Journal of Geophysical Research* 79: 4017–4028.

Helmberger DV and Harkrider D (1978) Modeling earthquakes with generalized ray theory. In: Miklowitz J and Achenbach JD (eds.) *Modern Problems in Elastic Wave Propagation*. New York: Wiley.

Helmberger DV, Zhao LS, and Garnero EJ (1996) Construction of synthetics for 2D structures, core phases. In: Boschi E and Ekstrom G (eds.) *Proceedings of International School of Solid Earth Geophysics: Seismic Modeling of the Earth's Structure*, pp. 183–222. Bologna, Italy: Società Italiana di Fisica.

Honda R and Yomogida K (2003) Static and dynamic displacement near a fault with the discrete wavenumber method. *Physics of the Earth and Planetary Interiors* 137: 107–127.

Holliger K, Levander A, and Goff JA (1993) Stochastic modeling of the reflective lower crust: Petrophysical and geological evidence from the Ivrea Zone (northern Italy). *Journal of Geophysical Research* 98: 11967–11980.

Igel H (1999) Modeling wave propagation in 3-D spherical sections by the Chebyshev spectral method. *Geophysical Journal International* 136: 559–567.

Igel H, Takeuchi N, Geller RJ, *et al.* (2000) The COSY Project: Verification of global seismic modeling algorithms. *Physics of the Earth and Planetary Interiors* 119: 3–23.

Imhof MG and Toksoz MN (2000) Multiple multipole expansions for elastic scattering. *Journal of the Acoustic Society of America* 100: 2969–2979.

Jeffreys H (1936) The structure of the Earth down to the 20 discontinuity. *Monthly Notices of the Royal Astronomical Society Geophysical Supplement* 3: 401–422.

Kaelin B and Johnson LR (1998) Dynamic composite elastic medium theory. Part II. Three-dimensional media. *Journal of Applied Physics* 84: 5488–5468.

Karato S-I (1993) Importance of anelasticity in the interpretation of seismic tomography. *Geophysical Research Letters* 20: 1623–1626.

Keith M and Crampin S (1977) Seismic body waves in anisotropic media: Reflection and refraction at a plane interface. *Geophysical Journal of the Royal Astronomical Society* 49: 181–208.

Kind R (1985) The reflectivity method for different source and receiver structures and comparison with GRF data. *Journal of Geophysics* 58: 146–152.
Kennett BLN (1983) *Seismic Wave Propagation in Stratified Media*. New York: Cambridge University Press.
Kennett BLN (1998) Guided-waves in three-dimensional structures. *Geophysical Journal International* 133: 159–174.
Kennett BLN (2001) *The Seismic Wavefield*, vols. I and II. New York: Cambridge University Press.
Komatitsch D and Vilotte J-P (1998) The spectral element method: An efficient tool to simulate the seismic response of 2D and 3D geological structures. *Bulletin of the Seismological Society of America* 88: 368–392.
Komatitsch D and Tromp J (1999) Introduction to the spectral-element method for 3-D seismic wave propagation. *Geophysical Journal International* 139: 806–822.
Komatitsch D and Tromp J (2002) Spectral-element simulations of global seismic wave propagation-II. 3-D models, oceans, rotation, and self gravitation. *Geophysical Journal International* 149: 390–412.
Korneev VA and Johnson LR (1993) Scattering of elastic waves by a spherical inclusion – I. Theory and numerical results. *Geophysical Journal International* 115: 230–250.
Kosloff D and Kessler D (1990) *Seismic Numerical Modeling: Oceanographic and Geophysical Tomography*, pp. 251–312. Amsterdam: Elsevier Science Publishers.
Langston CA and Helmberger DV (1975) A procedure for modeling dislocation sources. *Geophysical Journal* 42: 112–130.
Lapwood ER and Usami T (1981) *Free Oscillations of the Earth*. Cambridge, UK: Cambridge University Press.
Larsen S and Schultz CA (1995) ELAS3D: 2D/3D elastic finite difference propagation code, *Technical Report No. UCRL-MA-121792*, p. 19 Livermore, CA: Lawrence Livermore National Laboratory.
Li X-D and Tanimoto T (1993) Waveforms of long period body waves in a slightly aspherical earth model. *Geophysical Journal International* 112: 92–102.
Li X-D and Romanowicz B (1995) Comparison of global waveform inversions with and without considering cross branch coupling. *Geophysical Journal International* 121: 695–709.
Li X and Cormier VF (2002) Frequency dependent attenuation in the inner core: Part I. A viscoelastic interpretation. *Journal of Geophysical Research* 107, doi:10.1029/2002JB001795.
Masters G, Laske G, Bolton H, and Dziewonski A (2000) The relative behavior of shear velocity, bulk sound speed, and compressional velocity in the mantle: Implications for chemical and thermal structure. In: Karato S, Forte AM, Liebermann RC, Masters G, and Stixrude L (eds.) *AGU Monograph 117: Earth's Deep Interior*, pp. 63–86. Washington, DC: AGU.
Maupin V and Kennett BLN (1987) On the use of truncated model expansion in laterally varying media. *Geophysical Journal of the Royal Astronomical Society* 91: 837–851.
Maupin V (1989) Numerical modeling of Lg wave propagation across the North Sea Central Graben. *Geophysical Journal International* 99: 273–283.
Menke W and Richards PG (1980) Crust–mantle whispering gallery phases: A deterministic model of teleseismic Pn wave propagation. *Journal of Geophysical Research* 85: 5416–5422.
Menke W (2005) Case studies of seismic tomography and earthquake location in a regional context. In: Levander A and Nolet G (eds.) *Geophysical Monograph Series 157: Seismic Earth: Array Analysis of Broadband Seismograms*, pp. 7–36. Washington, DC: American Geophysical Union.
Müller G (1973) Amplitude studies of core phases. *Journal of Geophysical Research* 78: 3469–3490.
Müller G (1977) Earth-flattening approximation for body waves derived from geometric ray theory; improvements, corrections and range of applicability. *Journal of Geophysics* 42: 429–436.
Müller G (1985) The reflectivity method: A tutorial. *Journal of Geophysics* 58: 153–174.
Ni SD, Ding X, and Helmberger DV (2000) Constructing synthetics from deep Earth tomographic models. *Geophysical Journal International* 140: 71–82.
Olsen KB (2000) Site amplification in the Los Angeles basin from three-dimensional modeling of ground motion. *Bulletin of the Seismological Society of America* 90: S77–S94.
Rial JA and Cormier VF (1980) Seismic waves at the epicenter's antipode. *Journal of Geophysical Research* 85: 2661–2668.
Richards PG (1973) Calculation of body waves, for caustics and tunnelling in core phases. *Geophysical Journal of the Royal Astronomical Society* 35: 243–264.
Richards PG and Frasier CW (1976) Scattering of elastic waves from depth dependent inhomogeneities. *Geophysics* 41: 441–458.
Ritsema J and van Heijst HJ (2000) Seismic imaging of structural heterogeneity in Earth's mantle: Evidence for large-scale mantle flow. *Science Progress* 83: 243–259.
Robertsson JOA, Blanch JO, and Symes WW (1994) Viscoelastic finite-difference modeling. *Geophysics* 59: 1444–1456.
Rost S and Thomas C (2002) Array seismology: Methods and applications. *Reviews of Geophysics* 40, doi:10.1029/2000RG000100.
Sambridge M and Gudmundsson O (1998) Tomography with irregular cells. *Journal of Geophysical Research* 103: 773–781.
Shearer PM (1999) *Introduction to Seismology*. Cambridge, UK: Cambridge University Press.
Spudich P and Frazer LN (1984) Use of ray theory to calculate high-frequency radiation from earthquake sources having spatially variable rupture velocity and stress drop. *Bulletin of the Seismological Society of America* 74: 2061–2082.
Su W-J and Dziewonski AM (1997) Simultaneous inversions for 3-D variations in shear and bulk velocity in the mantle. *Physics of the Earth and Planetary Interiors* 100: 135–156.
Takeuchi N, Geller RJ, and Cummins PR (2000) Complete synthetic seismograms for 3-D heterogeneous Earth models computed using modified DSM operators and their applicability to inversion for Earth structure. *Physics of the Earth and Planetary Interiors* 119: 25–36.
To A, Romanowicz B, Capdeville Y, and Takeuchi N (2005) 3D effects of sharp boundaries at the borders of the African and Pacific superplumes: Observation and modeling. *Earth and Planetary Science Letters* 233: 137–153.
Trampert J, Vacher P, and Vlar N (2001) Sensitivities of seismic velocities to temperature, pressure and composition in the lower mantle. *Physics of the Earth and Planetary Interiors* 124: 255–267.
Virieux J (1985) SH-wave propagation in heterogeneous media: Velocity stress finite difference method. *Geophysics* 49: 1933–1957.
Virieux J (1986) P–SV wave propagation in heterogeneous media: Velocity–stress finite-difference method. *Geophysics* 51: 889–901.
Ward SN (1978) Long period reflected and converted upper mantle phases. *Bulletin of the Seismological Society of America* 68: 133–153.
Wen L and Helmberger DV (1998) A two-dimensional P–SV hybrid method and its application to modeling localized structures near the core–mantle boundary. *Journal of Geophysical Research* 103: 17901–17918.
Wu RS and Aki K (1985) Scattering characteristics of waves by an elastic heterogeneity. *Geophysics* 50: 582–595.

Zhao Y and Anderson DL (1994) Mineral physics constraints on the chemical composition of Earth's lower mantle. *Physics of the Earth and Planetary Interiors* 85: 273–292.

Relevant Websites

http://www.geodynamics.org – CIG, Computational Infrastructure for Geodynamics

http://www.eas.slu.edu – Computer Programs in Seismology, Department of Earth & Atmospheric Sciences, Saint Louis University.

http://www.geophysik.uni-muenchen.de – Geophysics, Department of Earth and Environmental Sciences, Ludwiq-Maximilians, University.

http://www.iris.edu – IRIS, Incorporated Research Institutions for Seismology.

http://www.ngdc.noaa.gov – NGDC Seismological Algorithms, USDOC/NOAA/NESDIS/National Geophysical Data Center (NGDC) Home Page.

http://www.orfeus-eu.org – Seismological Software Library, ORFEUS.

http://www.rses.anu.edu.au – Perspective Images of Slab Models by Oli Gudmundsson and Malcolm Sambridge, The RUM, ANU Research School of Earth Sciences.

http://sw3d.mff.cuni.cz – Seismic Waves in Complex 3-D Structures (SW3D), Charles University of Prague.

http://www.geom.uiuc.edu – The Geometry Center.